



TECHNICAL UNIVERSITY OF LIBEREC
Faculty of Mechatronics, Informatics
and Interdisciplinary Studies ■

Laser-mediated Synthesis of Iron Nanoclusters

Bachelor thesis

Study programme: B3942 – Nanotechnology
Study branch: 3942R002 – Nanomaterials

Author: **Ondřej Havelka**
Supervisor: M.Sc. Rafael Omar Torres Mendieta, Ph.D.





TECHNICKÁ UNIVERZITA V LIBERCI
Fakulta mechatroniky, informatiky
a mezioborových studií ■

Generování Fe nanoklastrů pomocí laseru

Bakalářská práce

Studijní program: B3942 – Nanotechnologie

Studijní obor: 3942R002 – Nanomateriály

Autor práce: **Ondřej Havelka**

Vedoucí práce: M.Sc. Rafael Omar Torres Mendieta, Ph.D.





Zadání bakalářské práce

Generování Fe nanoklastrů pomocí laserové syntézy

Jméno a příjmení: **Ondřej Havelka**
Osobní číslo: M16000109
Studijní program: B3942 Nanotechnologie
Studijní obor: Nanomateriály
Zadávající katedra: Katedra chemie
Akademický rok: **2018/2019**

Zásady pro vypracování:

1. The general goal of the thesis, is the synthesis of iron nanoclusters for its possible exploitation in the catalysis field, by using laser-mediated size reduction of micro and nanoparticles, an eco-friendly synthesis strategy.
2. To look for the optimal conditions that lead to the highest productivity rate of iron nanoclusters in terms of time and resources investment, by testing different laser fluences (at 3 different fluence regimens; high, threshold and low, where the threshold energy is going to be determined by means of a modification of the heating-melting-evaporation theory, the high energy will be » threshold value, and the low energy will be « threshold value), irradiation time, concentration of solid content in the liquid, testing of different fluids, etc.
3. Test the different physicochemical properties in the recently created advanced nanomaterials, looking for an outstanding behaviour derived from its low size.

Rozsah grafických prací: dle potřeby
Rozsah pracovní zprávy: 40-50 stran
Forma zpracování práce: tištěná
Jazyk zpracování práce: Angličtina



Seznam odborné literatury:

1. ZHANG, Dongshi; GOKCE, Bilal; BARCIKOWSKI, Stephan. Laser synthesis and processing of colloids: fundamentals and applications. *Chemical reviews*, 2017, 117.5: 3990-4103.
2. JIN, Rongchao, et al. Atomically precise colloidal metal nanoclusters and nanoparticles: Fundamentals and opportunities. *Chemical reviews*, 2016, 116.18: 10346-10413.
3. PYATENKO, Alexander, et al. Mechanism of pulse laser interaction with colloidal nanoparticles. *Laser & Photonics Reviews*, 2013, 7.4: 596-604.
4. BARCIKOWSKI, Stephan, et al. Handbook of laser synthesis of colloids. Universität Duisburg-Essen, 2016.
5. ANTONY, Jiji, et al. Synthesis and characterization of stable iron-iron oxide core-shell nanoclusters for environmental applications. *Journal of nanoscience and nanotechnology*, 2006, 6.2: 568-572.
6. FARRELL, Dorothy; MAJETICH, Sara A.; WILCOXON, Jess P. Preparation and characterization of monodisperse Fe nanoparticles. *The Journal of Physical Chemistry B*, 2003, 107.40: 11022-11030.
7. FRACASSO, Giulio, et al. Nanoaggregates of iron poly-oxo-clusters obtained by laser ablation in aqueous solution of phosphonates. *Journal of colloid and interface science*, 2018, 522: 208-216.

Vedoucí práce: Dr. Rafael Torres
Ústav nových technologií a aplikované informatiky
Datum zadání práce: 10. října 2018
Předpokládaný termín odevzdání: 30. dubna 2019

L. S.

prof. Ing. Zdeněk Plíva, Ph.D.
děkan

prof. Ing. Josef Šedlbauer, Ph.D.
vedoucí katedry

V Liberci 10. října 2018

Declaration

I hereby certify that I have been informed that Act 121/2000, the Copyright Act of the Czech Republic, namely Section 60, School-work, applies to my bachelor thesis in full scope. I acknowledge that the Technical University of Liberec (TUL) does not infringe my copyrights by using my bachelor thesis for TUL's internal purposes.

I am aware of my obligation to inform TUL on having used or licensed to use my bachelor thesis in which event TUL may require compensation of costs incurred in creating the work at up to their actual amount.

I have written my bachelor thesis myself using literature listed therein and consulting it with my supervisor and my tutor.

I hereby also declare that the hard copy of my bachelor thesis is identical with its electronic form as saved at the IS STAG portal.

Date:

Signature:

Abstract

In the current thesis, the main subject of study is the laser-mediated synthesis of iron nanoclusters. The process consists in reducing the size of iron microparticles by means of a photo-thermal evaporation effect prompted by nanosecond pulsed laser irradiation. The energy required to reduce the precursor element's size under 3 nm is determined by the theoretical model known as the particle heating-melting-evaporation model. The tested precursor colloid systems consist of iron microparticles with an average size of 2 μm dispersed in different polar solvents (water, methanol, ethanol, ethylene glycol and polyethylene glycol 400) and in liquid nitrogen. In order to deeply understand the technique, two different energy value regimes are used: lower and higher energy values than the threshold (depending on the liquid medium).

When energy values beyond the calculated threshold are used, it is possible to observe the successful synthesis of iron nanoclusters. Moreover, when the dipole moment of the used solvents is larger than the one found in water, the solvent seems to act as a capping agent enabling the stabilization of the produced nanomaterial without the use of external stabilization agents.

Finally, various optical and electron-based techniques are used to determine that the synthesized materials exhibit the expected optical and morphological properties. On top of, considering the material's outstanding characteristics indicated in the relevant literature, it is planned to test its catalytic activity and magnetic properties in the future.

Keywords: nanocluster, iron nanoparticle, iron, laser synthesis, pulsed laser, polar solvent, green chemistry

Abstrakt

V této bakalářské práci je zkoumána syntéza nanoklastrů železa, které jsou produkovány pomocí metody laserové syntézy. Syntetický přístup spočívá ve zmenšování velikosti železných mikročástic účinkem fototermálního vypařování vyvolaného ozařováním pomocí nanosekundového pulzního laseru. Energie potřebná k zmenšení velikosti prekurzních částic na průměrnou velikost pod 3 nm je určena teoretickým modelem známým jako model zahřívání-tavení-vypařování částic. Měřené prekurzorní koloidy jsou tvořené železnými mikročásticemi s průměrnou velikostí 2 μm , které jsou rozpuštěné v různých polárních rozpouštědlech (vodě, methanolu, ethanolu, ethylenglykolu a polyethylenglykolu 400) a v kapalném dusíku. Pro hlubší pochopení této techniky je použito dvou různých energií pro ozařování: podprahová a nadprahová hodnota energie (mění se v závislosti na kapalném médiu).

Při použití energie nad vypočtenou prahovou hodnotou je možné pozorovat úspěšnou syntézu nanoklastrů železa. V případě, kdy je dipólový moment použitých rozpouštědel větší než hodnota dipólového momentu vody, tak molekuly rozpouštědla obklopí částice, čímž umožní stabilizaci generovaného nanomateriálu bez použití přidaného stabilizačního činidla.

K určení a potvrzení očekávaných optických a morfologických vlastností syntetizovaných materiálů je použito optických a elektronových charakterizačních technik strukturní analýzy. Navíc s ohledem na další výjimečné charakteristiky materiálu, které jsou zmiňovány v související literatuře, je plánováno testování katalytických a magnetických vlastností materiálu.

Klíčová slova: nanoklustr, nanočástice železa, železo, laserová syntéza, pulsní laser, polární rozpouštědlo, udržitelná chemie

Acknowledgements

I would like to thank my thesis supervisor Rafael Omar Torres Mendieta, Ph.D. very much for his supervision, the engaging in the other scientific projects and especially for his rare inner peace during a long research work and his almost boundless openness to all my ideas. I am grateful to RNDr. Michal Řezanka, Ph.D. for the great recommendation to work with Rafael. I appreciate an opportunity to do research at the research center Institute for Nanomaterials, Advanced Technologies and Innovation (CxI) and regard the rest of laboratories collaborators for their helpfulness.

I would like to thank my family. My parents for their support during all my life. In particular, I am thankful to my mum for unpopular decisions which helped me in the past. Great thanks to my sister, who stood behind me when no one else understood me.

Moreover, I would like to thank my dorm roommate for our common enthusiasm for night trekking and my oldest friend for his absolute sincerity during last 19 years. Last but not least, I would like to thank my girlfriend for her light-hearted view of world.

Contents

List of abbreviations	9
List of figures	10
List of tables	11
1 Introduction	13
1.1 Nanoclusters	13
1.2 Fe nanoclusters	14
1.3 Ways to synthesize Fe nanoclusters	16
1.4 Laser-mediated synthesis	18
1.5 Laser fragmentation in liquids	21
2 Theoretical background	24
2.1 Heating-melting-evaporation model	24
3 Characterization techniques	28
3.1 UV-Vis spectroscopy	28
3.2 DLS	30
3.3 LDV	31
3.4 HR-TEM	32
3.5 ICP-OES	33
4 Setup details	35
5 Results	38
5.1 Preparation and synthesis	38
5.2 UV-Vis and fluorescence	39
5.3 DLS	41
5.4 LDV	43
5.5 HR-TEM	44
5.6 ICP-OES	46
6 Discussion	48
7 Conclusion	52
References	54

List of abbreviations

CCD	Charge-Coupled Device
CI particles	Carbonilazed Iron particles
CVC	Chemical Vapor Decomposition
cw	continuum wave
demiH₂O	Demineralized Water
DLS	Dynamic Light Scattering
EG	Ethylene Glycol
ESIONs	Extremely Small-sized Iron Oxide Nanoparticles
EtOH	Ethanol
FFs	Ferrofluids
FWHM	Full Width at Half Maximum
HRTEM	High-resolution Transmission Electron Microscope
ICP-OES	Inductively Coupled Plasma Optical Emission Spectroscopy
LDV	Laser Doppler Velocimetry
LFL	Laser Fragmentation in Liquids
LML	Laser Melting in Liquids
LPC	Laser Processing of Colloids
MeOH	Methanol
mol. wt.	molecular weight
MR fluids	Magnetorheological fluids
MRI	Magnetic Resonance Imaging
NCs	Nanoclusters
Nd:YLF	Neodymium-doped Yttrium Lithium Fluoride
NPs	Nanoparticles
PEG400	Polyethylene Glycol 400
PLAL	Pulsed Laser in Ablation in Liquids
QDs	Quantum Dots
SA:V	Surface-to-Volume ratio
SEM	Scanning Electron Microscope
SPR	Surface Plasmon Resonance
TEM	Transmission Electron Microscope
UV-Vis spectroscopy	Ultraviolet-Visible spectroscopy
XRD	X-ray Diffraction

List of Figures

1.1	Schematic illustration of the two groups of NPs synthesis strategies.	17
1.2	Number of citations per year determined by the ISI Web of Science search engine, while using the keywords “laser synthesis” and “nanoparticles”.	18
1.3	Schematic representation of PLAL technique divided into three steps: creation of a plasma due to the laser absorption, creation of a cavitation bubble after the transmission of the energy to the liquid medium and the final release of NPs to the liquid medium.	20
1.4	Schematic representation of LML technique divided into three steps: absorption of the laser radiation, melting and subsequent fuse of NPs and resultant nanocolloid composed by either nanomaterials with a single size or by nanomaterials with different morphology than the precursor one.	21
1.5	Schematic representation of LFL technique while using long laser pulses divided into four steps: laser irradiation, heating of the particles, creation of a cavitation bubble around the particle and final evaporation of the particle’s surface.	22
1.6	Schematic representation of LFL technique while using short laser pulses divided into three steps: laser irradiation, ejection of electrons and final coulomb explosion.	23
3.1	Simple schematic representation of a spectrophotometer, which is used to perform the UV-Vis spectroscopy measurements.	29
3.2	Scheme representing how the DLS instrument works.	31
3.3	Graphical illustration of the Zeta potential.	32
3.4	Minimal scheme of a HR-TEM instrument representing the parts described in the text.	33
3.5	Scheme of the basic elements of an ICP-OES spectrometer.	34
4.1	Experimental setup used for the synthesis of Fe nanoclusters with an energy fluence that exceeds the energy threshold required to evaporate the CI microparticles.	35
4.2	Experimental setup used for the synthesis of Fe nanoclusters with a lower energy fluence that the one required to evaporate the CI microparticles.	37

5.1	Fluorescence spectra of S4.	41
5.2	HR-TEM micrograph of sample S3 where it is possible to observe its crystalline nature.	46

List of Tables

5.1	List of samples used to synthesize Fe nanoclusters	38
5.2	List of fluence thresholds required to fully evaporate the CI microparticles. Both values obtained by means of the heating-melting-evaporation model.	39
5.3	List of UV-Vis spectra of the samples before the laser irradiation (Non-irradiated sample), after laser irradiation using a fluence value lower than the threshold value required to fully evaporate the microparticles (Below energy threshold) and after laser irradiation using the high fluence value (Beyond energy threshold). In addition, the graphs corresponding to the irradiated material include the spectra of the supernatant and the sediment.	40
5.4	List of DLS graphics.	42
5.5	List of hydrodynamic sizes, where M means maximum value of the size distribution and W refers to its width.	43
5.6	Zeta potential values	44
5.7	List of TEM images and size histograms of the supernatant of the corresponding samples irradiated at a high laser fluence.	45
5.8	Concentration of Fe measured by ICP-OES.	47
6.1	Colloidal behavior according to the Zeta potential values.	50

1 Introduction

Nanotechnology is daily presenting answer to the current and future problems of human kind. Since it was first discovered that nanomaterials (matter structured in the nanometric scale) exhibit non-conventional properties that are able to solve the hardest obstacles found in the nature, the scientific community has dedicated a great deal of effort to discovering all of the possibilities that nanoscience offers. [1, 2]

Among the most important instruments of the nanoscience, it is possible to identify the nanoparticles (NPs) as the building-blocks used to design *ad hoc* solutions. They consist of a set of atoms of the same or various chemical elements. The set is confined in a spatial region < 100 nm and the confinement provides an increment in the surface-to-volume ratio (SA:V), which means an enlargement of the population of atoms in the surface of the material that results in numerous phenomena, being the most important surface, coordination and quantum size effects. These phenomena lead to radical improvements of the materials towards various applications in comparison with their bulk counterpart.

In this context, the interest in the synthesis of NPs is constantly increasing. However, the main drawback of the NPs synthesis is the impossibility to get NPs of a single size. The properties displayed by the NPs are in a close relationship with their size. Thus, particles with various sizes might show a different behavior, making difficult to exploit in the most efficient way an specific property found in them.

Even when different attempts have been carried out to achieve the size monodispersity, the available synthesis pathways are often accompanied by the production of large quantities of waste and in the most of the cases no two NPs are the same. Therefore, the precise control over smaller dimensions is still a major case of study, which is how ultra-small NPs were developed (NPs with dimensions of < 3 nm). [3]

1.1 Nanoclusters

Among the different ultra-small NPs, those composed of metal are attracting a great deal of attention due to their potential applications in the photonic or electronic fields. Strictly, the metals with dimensions that are confined to the scale region under 2 nm are known as metal nanoclusters. [3, 4, 5] It is generally accepted that such materials may be perceived as constituent units that could lead to the further formation of common plasmonic NPs with sizes between 1 and 100 nm [6] or they may represent the intermediate step between single atoms and the NPs. [7]

According to the definition, a single nanocluster can contain from tens to several hundreds of atoms [8, 9] which may keep together due to weak forces (e.g. Van der Waals force) or by strong forces (e.g. ionic strength). [10] In addition, as the size of the nanoclusters is comparable with the Fermi wavelength of the electrons, their electronic band structure becomes discontinuous. Therefore, their behavior is similar to the one of the molecules and in consequence, some of the most common characteristics related to bigger systems are modified. This is the case of the Surface Plasmon Resonance (SPR) behavior displayed by noble-metal NPs which totally disappears when the size of the particles is lower than 2 nm. However in the counterpart, the combination of the discrete band structure and the ultra-small spatial confinement of nanoclusters causes the appearance of an important gap between the valence and conduction electrons enabling fluorescence emission as in the case of quantum dots (QD). [11, 12, 13, 14] Another important difference between the metal NPs and the nanoclusters can be observed in their chemical reactivity, as the SA:V found in the nanoclusters is larger in comparison with conventional NPs (the smaller diameter of the particles, the larger SA:V), the number of atoms located at their surface will also be larger maximizing in this way the reactive capabilities of the nanomaterial. [15]

In addition, there are some "disadvantages" associated with the ultra-small size of such materials, one of them is the reduction of their magnetic response which is a direct consequence of the lack of alignment of the spin in the atoms located at their surface, a phenomenon known as spin canting effect often found in small magnetic NPs. [16] Moreover, the electronic band structure modification that further leads to the previously mentioned quantum effects is highly dependent on the number of atoms in the structure and on its morphological shape. [3, 17]

Despite the different issues associated to their ultra-small size, the nanoclusters have been successfully used in a large number of applications displaying outstanding behaviours which in fact arise from their distinct properties in comparison with usual metal-based NPs and metals in bulk. [3] The specific optical, electric, magnetic, luminescent and reactive properties of the nanoclusters allow to use them in fields like biomedicine (e.g., cell labeling, cancer therapy, drug delivery, etc.) and catalysis (e.g., catalytic reduction or oxidation, electrocatalysis, photocatalysis, etc.). [18, 19, 20]

In this sense and considering the breakthrough impact that the use of nanoclusters is having in the nanoscience, which is reflected by an exponentially increasing rate of scientific papers dealing with the topic, it is the aim of the current thesis to explore and contribute to the issues related to the iron nanoclusters synthesis.

1.2 Fe nanoclusters

Among the different materials that nanoclusters can be composed of, iron (Fe) represents an interesting challenge. It attracts significant attention as it belongs to the group of materials that are considered environmentally and human friendly (depending on the amount of iron [21, 22]). The pure iron or the iron-based NPs

(e.g. iron oxides) are some of the most commonly synthesized NPs because there is a great interest in its superparamagnetic properties which in comparison with those coming from toxic materials as cobalt or nickel, can be efficiently exploited in various applications. In particular, in the biomedical field the magnetic properties of the Fe NPs enable their use as drug carriers or as diagnostic material. [23]

These properties do not represent the only reason why the Fe NPs are interesting, another remarkable properties include their catalytic outcomes, e.g., the reductive effect of the Fe NPs (especially of the nanoscale zero-valent iron) which is used for the remediation of the ground water from the pollutants, [24] and their use in information storage in which it is possible to take advantage of the magnetic properties of the material to accumulate information through their exposure to variable magnetisation patterns. [25]

As previously expressed, when the ultra-small size of nanoclusters is reached the properties of the material change. Surprisingly, the size reduction of Fe constitutes the next step in the improvement of the bulk material's properties, in contrast with the common Fe NPs, their larger SA:V promotes a higher catalytic effect. [26] In addition, the quantum effects of Fe nanoclusters could potentially lead to fluorescence, although this phenomenon has not been observed yet. In addition, when Fe oxide reaches the size of nanoclusters, it experiences a change in its magnetic properties allowing its use as a contrast agent in high resolution longitudinal relaxation magnetic resonance imaging (high resolution T_1 MRI).

To be more specific, the Fe oxide clusters, also known as extremely small-sized iron oxide NPs (ESIONs), exhibit a high r_1 (spin-lattice) relaxivity, which is related to a high number of unpaired electrons usually found in Fe oxide nanomaterials, and a low r_2/r_1 ratio derived from their low r_2 relaxivity. The r_2 (spin-spin) relaxivity is directly connected with the magnetic moment of the materials and this physical quantity is significantly decreased for the ultra-small magnetic NPs due to the decrement of the volume magnetic anisotropy and the spin disorders on the surface of the nanomaterial. On the contrary, the common-size iron oxide NPs exhibit a high r_2/r_1 ratio which makes them not suitable to be used as T_1 contrast agents but enables its use for the transversal relaxation MRI (T_2 MRI). However, the T_2 MRI represents a worse imaging method for taking high resolution images in comparison with the T_1 MRI due to the blooming effects or the possible confusions of hypointense areas.

For a long time, the gadolinium-based together with the manganese-based contrast agents were the most frequently used for the high resolution T_1 MRI. Nevertheless, the clinical applications show that such materials are quickly excreted through the urine and consequently decrease their circulating time in the human body which is unwanted for typical T_1 MRI long scan time. Moreover, they are very toxic and therefore dangerous for an excessive use. These issues do not concern the ESIONs, and therefore, their use is becoming more popular. [16]

The other sector in which Fe nanoclusters can have great implications is the smart fluids development. The smart fluids are understood as the type of liquids whose physical characteristics could be changed by the influence of an external magnetic or electric field. Among the different smart fluids, the two most notable

of them that greatly benefit from the inclusion of Fe are the magnetorheological fluids (MR fluids) and the ferrofluids (FFs). On the one hand, the FFs are strongly magnetizable and stable colloids that encompass the use of sub-domain magnetic 3-15 nm particles. On the other hand, the MR fluids are colloids whose phase can be controlled by a magnetic field, they are composed by multi-domain ferro- or ferrimagnetic particles with sizes of 1-20 μm dispersed in organic oils.

These two-phase fluids are of great interest because they allow an up to thousand times increase in their viscosity in fractions of seconds, making them attractive for various applications in the sectors of material science (e.g. dope liquid crystals with magnetic particles), technology (e.g. inertial and viscous damping, heat dissipation and dynamic sealing), biomedicine (e.g. hyperthermia, drug delivery and targeting, separation of cells and before mentioned MRI contrast), etc. [27, 28]

Despite the potential of such smart fluids, it was recently found that the use of particles with a monomodal size distribution may represent a problem, especially in the case of MR fluids, where this characteristic leads to the lose of their magnetic and rheological properties. [29, 30] One of the ways to alleviate this issue is by the use of small particles which causes an increment of dipolar interaction, relating significantly to the magnetic and repulsion force and thus allowing the decreasing of aggregation and sedimentation of microparticles. [29]

The production of high quality FFs and MR fluids is of great importance because it may enable the study of their properties and its further exploitation in an even larger variety of applications.

Finally, it is worth to mention that even when great applications are envisaged for the use of Fe nanoclusters, the potential of the material has not been extensively explored. There are not many studies related to the synthesis of Fe nanoclusters, and therefore, it is a priority to contribute to and to extend the knowledge in the field.

1.3 Ways to synthesize Fe nanoclusters

The fabrication of precise nanostructures requires a high control over the size, shape, chemical structure, functionalization and properties resulting therefrom. For this, several synthesis pathways have been developed through the latest years, which can be divided into two big groups: the top-down and the bottom-up techniques (see Fig. 4.1). By definition, the top-down synthesis strategies are those in which a bulk material is turned into small pieces reaching the size of nanometers. The bottom-up techniques are those in which the nanomaterial is generated by the self assemble of its constituent components. Despite these definitions, some methods are considered as being simultaneously a top-down and a bottom-up technique. It depends on the processes which are in progress during the fabrication. [31]

In this context, several of these techniques have been used to synthesize Fe NPs with sizes over 10 nm, the most common of which being the severe plastic deformation, pulse electrodeposition, gas-phase reduction, liquid phase reduction and liquid flame spray. [32] The techniques which push the limits of the miniaturization

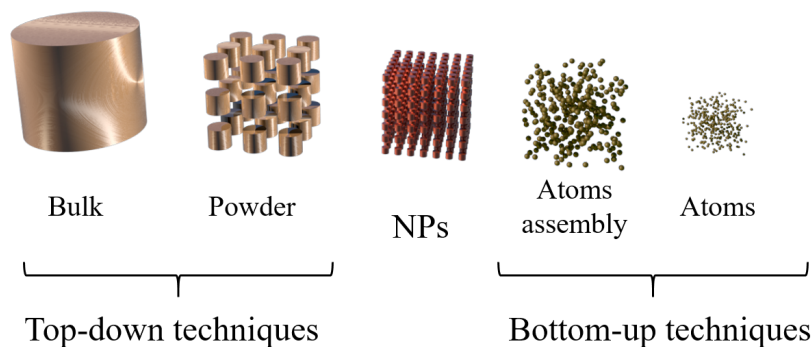


Figure 1.1: Schematic illustration of the two groups of NPs synthesis strategies.

of Fe NPs reaching sizes around 10 nm are: inert gas condensation, hydrothermal synthesis, high-energy ball milling and ultrasound shot peening.

In the framework of this thesis, not many attempts have been done to reach the ultra-small size of the nanoclusters (below 2 nm). However, the most explored techniques towards reaching such sizes are: thermal decomposition, controlled chemical coprecipitation, microemulsion (or reverse micelle) synthesis method and chemical vapor condensation. [33, 34, 35]

The thermal decomposition technique allows to synthesize Fe NPs with a highly uniform size distribution while using non-toxic and relatively cheap precursors. Furthermore, the size of particles could be easily modified by changing the reaction conditions, making possible to reach structures with few nanometers. [16, 34] The controlled chemical coprecipitation is considered an economically-effective and bio-compatible technique for the synthesis of fairly well uniform crystalline Fe NPs, and even when the shape of the final product is difficult to control in comparison with thermal decomposition, it is feasible to synthesize nanomaterials with a size of 2-4 nm. The biggest advantage of this method is the fabrication rate which in comparison with thermal decomposition, that takes hours, takes minutes. [35, 36] The microemulsion technique is used for the synthesis of Fe-M based NPs, where M means any metal that may be part of the final structure of the particle, such as cobalt, manganese, etc. The fabrication process is complicated in comparison with the previously mentioned thermal decomposition and controlled chemical coprecipitation techniques. Moreover, its fabrication rate is low and consequently also economically low-effective. [35] The chemical vapor condensation (CVC) is based on the pyrolysis of organometallic precursors to allow the fabrication of Fe NPs with sizes that may reach 6 nm. The disadvantage of this technique is the relatively wide size distribution of particles. [37]

In addition, the most substantial issues related to all of those techniques are the necessity to use hazardous chemicals for the successful fabrication of the material and the production of large amounts of chemical waste. In response to these problems, the combination of nanoscience and optics has brought different interesting alternatives, among which, laser synthesis of colloids (LSC) is becoming extremely popular due to its versatility, safeness and degree of reproducibility. This is demonstrated

by the exponentially increasing number of citation when searching the keywords “laser synthesis” and “nanoparticles” in the ISI Web of Science, a searching engine that enables an access to a set of bibliographic resources and databases that cover all the fields of the academic knowledge (Fig. 1.2).

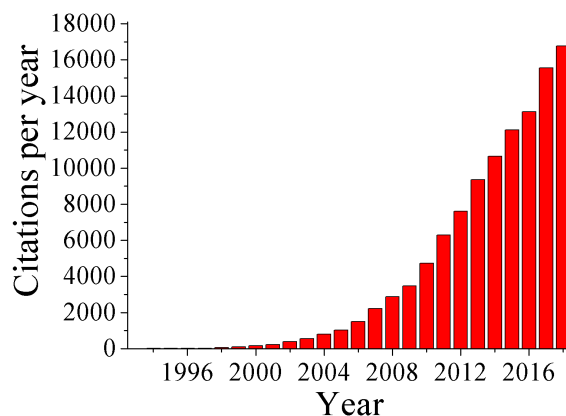


Figure 1.2: Number of citations per year determined by the ISI Web of Science search engine, while using the keywords “laser synthesis” and “nanoparticles”.

The LSC strategy has been many times successfully applied in the fabrication of Au, Ag and other material nanoclusters, but not yet extensively exploited in the production of Fe nanoclusters. Up to date the only study reported about it, is the synthesis of nanoaggregates of Fe nanoclusters performed by Amendola et. al. [38]

1.4 Laser-mediated synthesis

In general, in the LSC technique a laser source is used to irradiate a bulk material that is immersed in a liquid environment. The interaction between the light and the matter leads to the miniaturization of the bulk material resulting in the fabrication of a colloid composed by NPs that may even reach sizes under 10 nm. [39]

Since the first reports in the late 80’s and early 90’s, [40, 41] the technique demonstrated a great potential to overcome the current issues related to the conventional synthesis approaches, allowing to get a wide variety of nanomaterials in a clean and safe way, [42] and therefore consequentially, to replace the hazardous external reducing agents by the laser radiation. In addition, as the technique is compatible with the use of macromolecules or monovalent salts, it is possible to manufacture stable and complex nanostructures. [43] Moreover, the nanomaterials produced by LSC have a significantly higher purity and the method adhere to the principles of the “green” chemistry. [42]

By definition, a methodology used to fabricate nanomaterials agrees with the principles of the “green” chemistry when it avoids environmental detrimental effects and reduces the use and the generation of hazardous substances, which is one of the biggest challenges in the modern science. [44]

Despite the benefits, there are some issues connected with the LSC e.g., the low mass productivity and the impossibility to directly synthesize organic NPs due to the possible incineration of the organic bulk material. In terms of cost, the laser-mediated method is still behind the conventional chemical techniques. In a long-term view, considering the great advances in the laser science, it could be expected that the LSC technique gets cheaper and more popular due to its larger versatility in comparison with the traditional methodologies. [42]

Regarding the laser sources exploited in LSC, it is possible to use two basic types: continuum wave lasers (cw-lasers) and pulsed lasers. As their name indicates, the cw-lasers are delivering a beam of coherent and high energetic electromagnetic waves continuously and the pulsed lasers are delivering such beams in trains of pulses, where each pulse confines a huge population of photons making possible to reach peak powers in the scale of hundreds of GW.

Towards LSC, while using cw-lasers, where the incoming beam is composed by a low population of photons that are delivered continuously, the photons are absorbed by the irradiated material and further distributed through the whole material in the form of vibrations. After the accumulation of the energy, it is possible to surpass the threshold energy of the material to break its cohesion and finally achieve its miniaturization. Even when cw-lasers can reach huge amounts of power and are conventionally used in the laser- engraving and -drilling sectors, for LSC, it is preferred to use pulsed laser sources because in a liquid environment the cw-lasers may transfer huge amounts of energy to the bulk material and this in turn will transfer the energy to the liquid leading to its fast evaporation and eventually to the destruction of the colloid.

In contrast, a pulsed laser is almost ideal for the LSC. In a pulsed laser source, the coherent and high energetic electromagnetic waves are not continuously delivered but are rather compressed in packages of time and released at an specific repetition rate allowing to deliver huge concentrations of photons in fractions of seconds. Then, the energy absorbed by the bulk material can be enough to surpass the threshold necessary for the miniaturization and no accumulation of energy is present. Thus, the energy is not largely transferred to the liquid and the final form of the product can be colloidal. [45]

The pulsed laser sources that are conventionally used in LSC are those with a pulse width in the temporal region of the nanoseconds, picoseconds and femtoseconds (ns or 10^{-9} s, ps or 10^{-12} s and fs or 10^{-15} s). As it may be expected, the shorter the pulse width, the higher the peak power and thus, the higher the chances to surpass the threshold energy towards the material's miniaturization.

In general, the last statement is true. However, when performing LSC there are some conditions behind the use of each pulse width, i.e., while using ps or fs, it is possible to deliver a large population of photons in shorter time than the electron-phonon relaxation time (in the region of ps). [46] Therefore, the miniaturization of the bulk material may be preferentially conducted through non-linear optical phenomena as multi-photon ionization, in which the incoming energy is insignificantly transferred to the rest of the material and used to detach the irradiated area out of the bulk. Nevertheless, as the energy confined in such short pulses is extremely

large, the liquid can also undergo the non-linear optical phenomena avoiding the laser beam effectively reaches the solid bulk target.

In contrast, the ns pulses are longer than the electronic relaxation time and the miniaturization is rather promoted by thermal effects because the non-linear optical phenomena are not as efficiently reached as in the case of ps and fs. However, the ns pulses are not as long as the energy gets largely transmitted to the liquid environment. Therefore, in LSC the majority of the energy is effectively used to achieve the miniaturization of the solid bulk material.

Essentially, LSC can be divided into three different approaches and for each one a different pulsed laser source is preferred: the pulsed laser ablation in liquids (PLAL), laser melting in liquids (LML) and laser fragmentation in liquids (LFL), which are different from each other due to the physical and chemical processes during their course.

PLAL consists in irradiating a 3 dimensional bulk solid immersed in a liquid environment with a focused pulsed laser beam, which is immersed in a liquid environment. The laser-matter interaction leads to the release of little pieces from the bulk in the form of a plasma. Later the material detached out of the bulk might be enclosed in a cavitation bubble created around the area of the irradiation due to the transfer of energy from the irradiation point to the liquid. Subsequently, the cavitation bubble collapses and releases particles into the surrounding liquid environment, resulting in the colloid (Fig. 1.3). The pulsed laser source that is preferred for PLAL is a ps laser emitting radiation at wavelengths from 800 to 1064 nm.

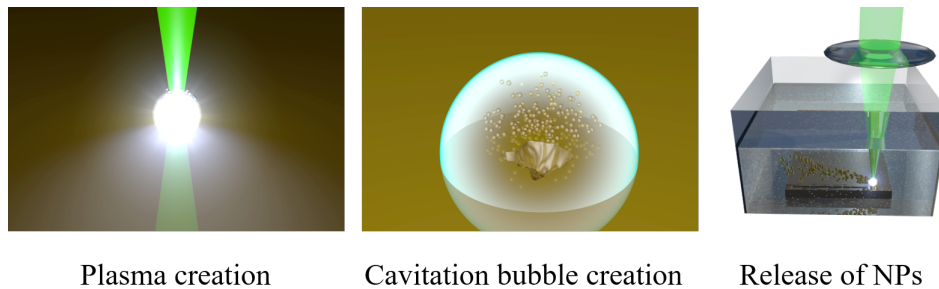


Figure 1.3: Schematic representation of PLAL technique divided into three steps: creation of a plasma due to the laser absorption, creation of a cavitation bubble after the transmission of the energy to the liquid medium and the final release of NPs to the liquid medium.

Differently, LML is a photothermal technique used to the growing or reshaping of the NPs morphology. In detail, a non focused or barely focused laser beam is used to irradiate NPs immersed in a liquid environment. The large population of photons that is confined in the incoming laser pulses (often in a temporal window of ns) is absorbed by the electrons of the atoms that belong to the NPs, later the absorbed energy is distributed through the whole electronic lattice of the NPs through vibrations, allowing the NP to melt-down. When the NPs reach a melting temperature, they can fuse with each other, enabling in this way to generate NPs

of a homogeneous size distribution or to change the shape of NPs into nanorods, nanochains, nanospheres, etc. (Fig. 1.4).

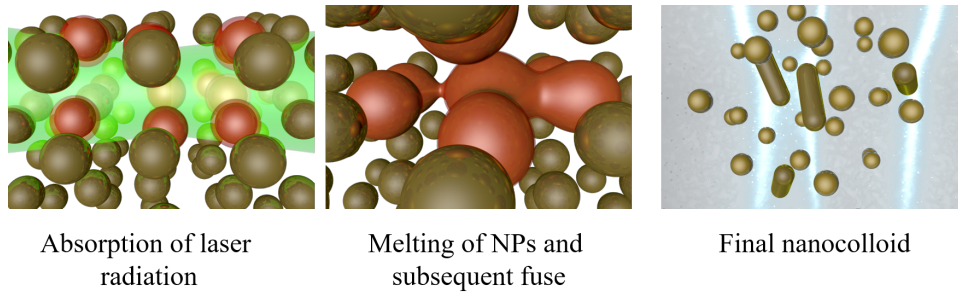


Figure 1.4: Schematic representation of LML technique divided into three steps: absorption of the laser radiation, melting and subsequent fuse of NPs and resultant nanocolloid composed by either nanomaterials with a single size or by nanomaterials with different morphology than the precursor one.

Finally, LFL uses a similar setup as the one of LML, but the biggest difference between each other is the amount of energy used. While LML uses a non focused or barely focused laser beam, in LFL it is mandatory to focus the laser beam in order to confine the delivered energy in time and also in space to reach the explosion or evaporation of micro or sub-micrometric particles enabling the generation of ultra-small NPs.

1.5 Laser fragmentation in liquids

The LFL technique is divided into two pathways, thermal and non-thermal. The difference between them is associated with the laser pulse length. The thermal effects take place when the laser pulse duration is longer than several ps and the non-thermal effects are exhibited when the pulse length is shorter than few ps. The classification of pathways arises from the electron-phonon relaxation time. As previously mentioned, the relaxation time represents the interval which an electron needs to go back from an excited to a basal energy state and conventionally subsist around the level of 10^{-12} s. [46, 47]

On the one hand, when lasers with a long pulse width are used, a photothermal evaporation process may occur. In this situation, a laser pulse interacts with the surfaces of targeted particles for a long-time interval, specially, the photons in a laser pulse bombards the solid material long enough to allow the release of vibration energy from the single atomic systems and the released energy is absorbed by the surrounding systems. [48] The phenomena of energy transmission thanks to the vibrations allows good energy distribution in the whole surface of the particle leading firstly to its melting and eventually, with enough energy, to its evaporation (Fig. 1.5). [49]

The process of evaporation can differ depending on the energy of the laser pulse. If the energy of laser pulse is too low and the temperature of the particles is below the

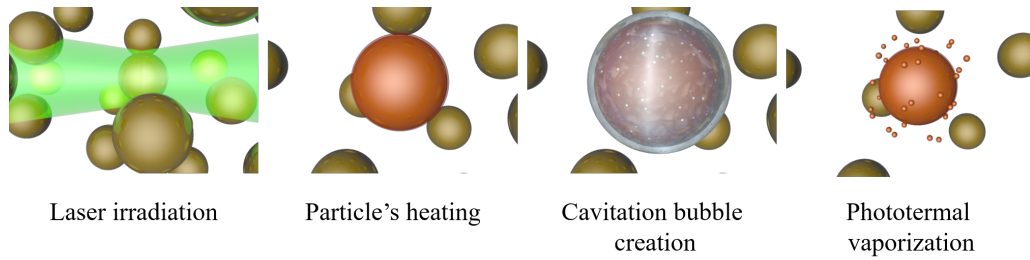


Figure 1.5: Schematic representation of LFL technique while using long laser pulses divided into four steps: laser irradiation, heating of the particles, creation of a cavitation bubble around the particle and final evaporation of the particle's surface.

melting point, only the photothermal reshaping happens. In contrast, if the energy of the laser pulses is too high, it may cause the explosive evaporation together with before mentioned surface evaporation. The temperature of particles for this phenomenon goes up to the boiling temperature. Last but not least, the evaporation phenomena is significantly connected to the creation of a cavitation bubble around the irradiated particle due to the release of energy from particle to the liquid. The electron-phonon relaxation allows the liquid heating to the spinodal temperature, i.e., higher temperature than the boiling temperature, thus the state of the medium is changed to the gas. In that moment, the gas enclose the particles in the forming cavitation bubble, which is believed to act as a reactor for the final formation of small NPs. [50]

On the other hand, when shorter pulse lengths are used, the fragmentation of bigger particles may occur due to Coulomb explosion and photo-dissociation, both phenomena being a consequence of the detachment of electrons and ions out of the material's surface due to the multiphoton absorption. As previously expressed, the multiphoton absorption happens because while electrons still do not go back from their excited state to the basal state, they already interact with more photons concentrated in temporal regions that are shorter than the conventional electron-phonon relaxation time. Finally, leading to the complete detachment of the electrons out of their atomic system, leaving a system with a lack of electrons that by the interaction with the neighbor atomic systems might be forced to leave the bulk material. Reaching in this way the miniaturization of the irradiated material (Fig. 1.6). [51, 52]

Regardless the length of the laser pulses, the laser fragmentation efficiency get incremented with increasing laser energy per irradiated surface (laser fluence) but the density of the energy must be below the threshold of the liquid breakdown and other undesirable nonlinear optical effects decreasing the efficiency and making the control of NPs synthesis difficult. [42]

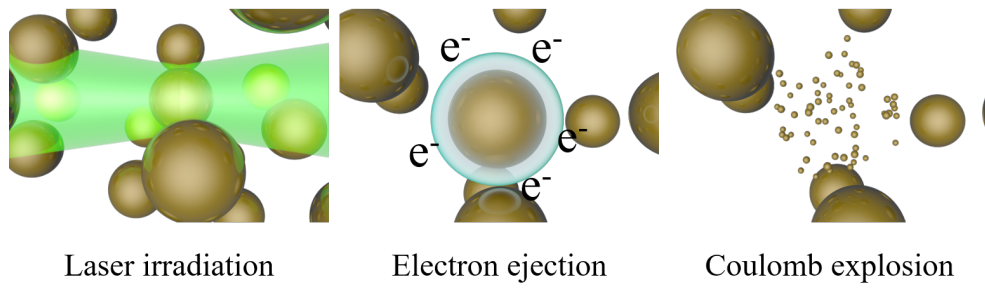


Figure 1.6: Schematic representation of LFL technique while using short laser pulses divided into three steps: laser irradiation, ejection of electrons and final coulomb explosion.

2 Theoretical background

While using LFL, the laser fluence is one of the most important conditions which has a direct influence on the size of the final generated particles. The synthesis of smaller particles occurs when the energy threshold is overcome and thus the particles succumb to fragmentation.

In this context, the calculation of the energy threshold for the different materials is needed. This is conventionally done by using the heating-melting-evaporation model originally formulated in 1999 by Koda et.al. [53] and further developed by Pyatenko et.al. [54] The model has been successfully used to determine the final size of the fabricated particles in numerous experiments. [55, 56] The model presupposes that all the energy coming from the laser radiation that is absorbed by the bulk material is used in the heating-melting-evaporation process. [48]

Up to date, the full structure of the heating-melting-evaporation model leads to the disclosure of the energetic thresholds needed to promote the heating, the melting, the evaporation of the surface of sub-micrometric particles or their complete evaporation. [50]

In the thesis, the model is used to identify the energy thresholds at which the bulk materials undergo a complete evaporation, not only of their surface but rather of their entire three dimensional structure, reaching in this way the ultra-small size of the nanoclusters. In addition, the mathematical expressions in the model are adapted for the needs of the presented experiments.

2.1 Heating-melting-evaporation model

The heating-melting-evaporation model describes the following situation: a laser beam (one laser pulse) interacts with micrometric or sub-micrometric particles immersed in a liquid environment, the particles absorb all of the incoming energy which is used to heat them up. Subsequently, the particles are heated up to a specific temperature needed for the transformation of the material's state.

In the theoretical model, the energy absorbed by the particles is equal to

$$E_{abs} = \frac{E_0}{S_0} \cdot \sigma_{abs} = \Psi \cdot \sigma_{abs} \quad (2.1)$$

where E_0 represents the energy of a single pulse, S_0 the laser beam cross section (the area of light that is perpendicular to the beam direction), $\Psi = E_0/S_0$ the laser

fluence and σ_{abs} the particle absorption cross section which describes the energy absorbed by the irradiated particle.

Although the σ_{abs} depends on the shape of each particle, the calculations consider an ideal situation in which all the irradiated particles are spherical. The conventional way to get this value is through the use of the Mie theory which describes the interaction between a sphere and a planar electromagnetic wave. Nowadays, there are many Mie calculators available that allow to get this value in an easily way. [57] These calculators need some input data about the irradiated material and the surrounding medium, such as the refractive index and the extinction coefficient of the bulk material, the refractive index of the medium, the sphere diameter and the interval of wavelengths in which the sphere may be irradiated.

Therefore, the σ_{abs} value is significantly influenced by the particle size and the wavelength of the laser used for the irradiation. In the current thesis, the used laser wavelength is 527 nm which is suitable in terms of significant light interaction with the studied material. [50]

After knowing the σ_{abs} , it is possible to determine the amount of energy absorbed by a single particle of any size using the equation 2.1. According to the model, the energy of the laser pulse is completely absorbed by the solvated particles in the medium and transformed into heat. This changeover is simplified as a complete 100 % transformation. Thus, the equation can be written as the energy absorbed by one particle being equal to the received heat which can be expressed in terms of the weight of the material and its temperature dependent heat capacity c_p

$$\Psi \cdot \sigma_{abs} = m_p \cdot \int_{T_0}^T c_p(T) \cdot dT \quad (2.2)$$

where $m_p = \rho_p \pi d_p^3 / 6$ is the particle mass, ρ_p is the density of the particle, d_p is the diameter of the particle and T_0 is the initial temperature of the particle and T is the final temperature of the particle. Consequently, when the laser radiation heats up the particle until the point of its melting temperature, the melting of the solid structure might occur. However, if the radiation exceeds this temperature level the excess of energy might be used for a further increment of temperature of the particle in the “liquid state”, i.e., keeping as a quasi-spherical droplet that holds together due to surface tension promoted by the liquid surrounding medium. If the temperature reaches the boiling point of the irradiated material, the “particle” will be in a state known as full melting. This is the point used for the LML synthesis technique, in which the melting of the particles is used to fuse the precursor material into bigger particles or particles with various morphologies. However, when the laser irradiation surpass this temperature value, the particle in the liquid state may undergo a vaporization process, being the surface of the material the one that vaporize first but if the vaporization temperature point is largely exceeded, the particle may reach a full-evaporation.

The final expression of the heating-melting-evaporation model can be described in a similar form as the before mentioned equation of heating (eq. 2.2). The equation parts that are associated to the transformation of the states of matter are represented by enthalpies per mass (ΔH) which can be found in different tables or calculated

from the enthalpy per moll values for each material.

$$\Psi \cdot \sigma_{abs} = m_p \cdot \int_{T_0}^{T_m} c_p^s(T) \cdot dT + m_p \cdot \Delta H_m + m_p \cdot \int_{T_m}^{T_b} c_p^l(T) \cdot dT + m_p \cdot \Delta H_{ev} \quad (2.3)$$

Here, c_p^s represents the heat capacity of the material in the solid state, c_p^l the heat capacity in the liquid state, T_m the melting temperature, T_b the boiling temperature and as previously mentioned, ΔH_m the enthalpy of the melting and ΔH_{ev} the enthalpy of the evaporation. Finally, if the final temperature of the irradiated particles is a known value or when a significant temperature (melting or boiling temperature) is reached, the integral section of the temperature dependent of the heat capacities in the equation 2.3 can be replaced by the enthalpy per mass corresponding to the given temperatures, as it is described in the following expression

$$\Psi \cdot \sigma_{abs} = m_p \cdot [(H_{T_m} - H_{T_0}) + \Delta H_m + (H_{T_b} - H_{T_m}) + \Delta H_{ev}] \quad (2.4)$$

where $H_{T_m} - H_{T_0}$ represents the relative enthalpy to reach the melting point and $H_{T_b} - H_{T_m}$ the relative enthalpy to reach the boiling point.

Therefore, the equation 2.4 can be used to calculate the threshold fluence required to reach the heating, the melting, the boiling and the evaporation of micro or sub-micrometric particles. However, if the goal is to reach not only the surface evaporation of the particles, but instead their complete evaporation, it is important to consider that after the boiling point the particles will receive more and more energy increasing their temperature until they start to evaporate, and therefore, decreasing their size. Thus, the particle absorption cross section also will decrease during the evaporation process and a larger energy may be necessary to keep evaporating the material. Then, the fluence value required to fully evaporate the material will be determined by the integral of the following differential equation describing the evolution of the absorption cross section in terms of the particle's size during the evaporation

$$\sigma_{abs}(d_p) \cdot \mathbf{d}(\Psi) = \Delta H_{ev} \cdot \mathbf{d}(m_p) \quad (2.5)$$

which after the substitution of m_p and the editing takes the following form

$$\mathbf{d}(\Psi) = \frac{\pi}{2} \cdot \rho_p \cdot \Delta H_{ev} \cdot \frac{d_p^2 \cdot \mathbf{d}(d_p)}{\sigma_{abs}(d_p)} \quad (2.6)$$

Then, the final equation that enables to calculate the required fluence to fully evaporate micro or sub-micrometric particles will be

$$\begin{aligned} \Psi = & \frac{\pi \cdot d_p^3 \cdot \rho_p}{6 \cdot \sigma_{abs}} \cdot [(H_{T_m} - H_{T_0}) + \Delta H_m + (H_{T_b} - H_{T_m})] + \\ & \frac{\pi \cdot \rho_p}{2} \cdot \Delta H_{ev} \cdot \left(\int_{d_p}^0 \frac{d_p^2}{\sigma_{abs}(d_p)} \cdot \mathbf{d}(d_p) \right) \end{aligned} \quad (2.7)$$

In addition, in the thesis the equation is enriched by considering that the laser beam may lose energy throughout its pathway by interacting with the colloid before reaching the focal point where the desired irradiation of particles occurs. The way to include the loss of energy is simply by multiplying the theoretical fluence $\Psi_{theoretical}$ with the transmittance T_λ of the laser radiation after passing through a specific colloid pathway, as expressed in the following equation

$$\Psi_{real} = \Psi_{theoretical} \cdot T_\lambda \quad (2.8)$$

In this sense, we compensate in a rough way the possible energy losses that we may get while the laser passes through the liquid by increasing the real fluence used Ψ_{real} . Thus, the final equation is

$$\Psi_{real} = \frac{\pi \cdot \rho_p}{2 \cdot T_\lambda} \left[\frac{d_p^3}{3 \cdot \sigma_{abs}} \cdot [(H_{T_m} - H_{T_0}) + \Delta H_m + (H_{T_b} - H_{T_m})] + \Delta H_{ev} \cdot \left(\int_{d_p}^0 \frac{d_p^2}{\sigma_{abs}(d_p)} \cdot \mathbf{d}(d_p) \right) \right] \quad (2.9)$$

Finally, note that in the current model it is assumed that there are not heat losses while the process is taking place. This assumption is correct when a ns pulsed laser beam is used to promote the full evaporation of the particles, as it is in the thesis, but may not be correct if the pulse duration of the laser exceeds the time required for the cooling and solidification of the particles (from 10^{-5} s to 10^{-6} s), which is believed to be one of the principle processes that may promote the heating loose through conductive/convective heat transfer between the particle and the liquid. [48]

Therefore, if the experiments reported herein are planned to be reproduced, it is important to keep in mind that the described model may work only for pulsed laser sources with a pulse length shorter than 10^{-6} s.

3 Characterization techniques

The materials produced in the thesis are characterized by means of the following techniques: ultraviolet-visible spectroscopy (UV-Vis spectroscopy), high-resolution transmission electron microscopy (HR-TEM), dynamic light scattering (DLS), laser doppler velocimetry (LDV) and inductively coupled plasma optical emission spectrometry (ICP-OES).

Each characterization technique allows to analyse specific information about the synthesized material. In the case of UV-Vis spectroscopy, the technique is used to determine the absorption spectra of the samples, which is important to define if the samples display outstanding optical properties, such as fluorescence or SPR activity. Moreover, in combination with the Mie calculators, the technique is used to roughly estimate the size of the synthesized particles.

The DLS technique is used to ratify the size of the nanomaterial by the measurement of the hydrodynamic size of the NPs while dispersed in the liquid medium.

The LDV technique is used to measure the Zeta potential of the material, a value that indicates how stable a colloidal suspension can be.

The HR-TEM technique is used to observe the size, shape and crystallographic structure of the particles. This technique is extremely precise and if it is properly used, it allows to analyse a fare statistical fragment of the material. However, to determine the correct size of the produced material it is necessary to use it in combination with a technique that allows to measure the material in a more general way, such as DLS does.

Finally, the ICP-OES technique is used to determine the percentage of individual chemical elements found in the fabricated samples, a value that enables to determine the production efficiency of the technique, among other things.

3.1 UV-Vis spectroscopy

The UV-Vis spectroscopy measurements were carried out by the use of a spectrophotometer (Hach-Lange, DR6000, wavelength range from 190 to 1100 nm) that has a wavelength resolution of 0.1 nm. The instrument is equipped with two light sources, a deuterium lamp covering the UV spectrum (190 to 360 nm) and a halogen lamp covering the visible spectrum (390 to 1100 nm). The light coming from the lamps is separated into its composing wavelengths by the use of a diffraction grill. Furthermore, each wavelength is separately irradiating a colloidal sample in a transmission disposition, as displayed in Fig. 3.1.

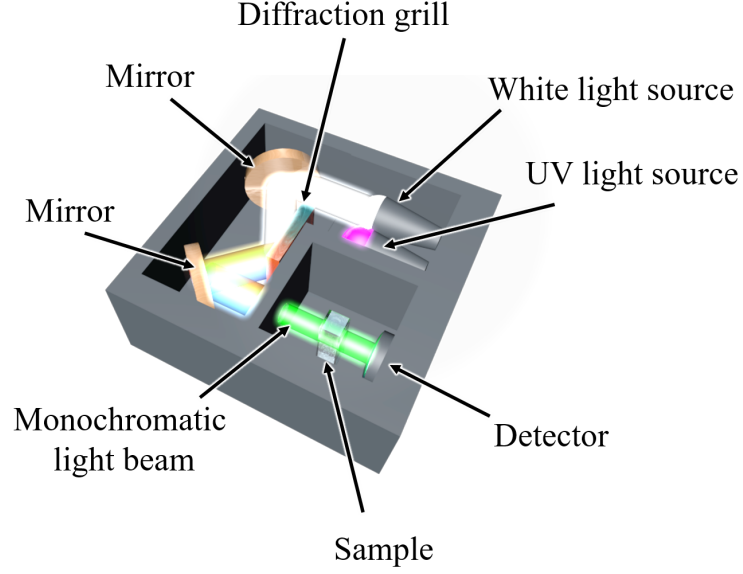


Figure 3.1: Simple schematic representation of a spectrophotometer, which is used to perform the UV-Vis spectroscopy measurements.

After the light propagates through the colloidal sample, the outgoing light is collected by a detector comparing the measured light intensity with the incoming one, allowing to determine in this way the transmittance of the light and after the following relations the absorbance of the light

$$T_\lambda = \frac{I}{I_0} \quad (3.1)$$

$$A = -\log_{10}(T_\lambda) = -\log_{10}\left(\frac{I}{I_0}\right) = \frac{\ln(e^{\alpha(\lambda)d})}{\ln(10)} = \frac{\alpha(\lambda)d}{2.3} \quad (3.2)$$

where I_0 is the incoming light intensity, I is the measured light intensity, λ is the wavelength, α is the absorption coefficient and d is the optical path in which the light interacts with the colloidal sample.

Therefore, by measuring the light transmittance it is possible to determine different optical characteristics of the samples under study. Being the most important for our purposes the amount of absorption of a specific wavelength.

In addition, the determination of the size is assessed by considering the classical Mie theory for the case of the interaction between a homogeneous metallic nanosphere and a planar electromagnetic wave. In the presence of the wave's electromagnetic field, the sphere may absorb and scatter light in the way of the following set of relations

$$C_{ext} = \frac{24\pi^2 R^3 \epsilon_d^{3/2}}{\lambda} \frac{\epsilon_m''}{(\epsilon_m' + 2\epsilon_d)^2 + (\epsilon_m'')^2} \quad (3.3)$$

$$\epsilon'_m = \epsilon^\infty - \frac{w_p^2}{w^2 + \gamma^2} \quad (3.4)$$

$$\epsilon''_m = \frac{w_p^2 \gamma}{w(w^2 + \gamma^2)} \quad (3.5)$$

$$\gamma = \frac{\nu_F}{L_{bulk}} \quad (3.6)$$

where C_{ext} represents the extinction coefficient of the particle, often equal to the addition of the absorption and scattering values. R representing the radius of the particle, ϵ_d its dielectric function, ϵ_m the dielectric function of the medium in which the particle can be immersed, ϵ^∞ the dielectric function at high frequencies (it can be considered 1 for the most of the materials), w the frequency of the incoming light, w_p the frequency at which the electrons in the NPs resonate with the incoming light, ν_F the velocity of Fermi and L_{bulk} the pathway of the electrons in the bulk material.

These relation can be used to fit the absorbance spectra of the samples and disclose the size of the particles in a colloidal sample. As expressed in third chapter, in the thesis the Mie calculators applying these relations are used to compare their results with the absorption spectra of our samples.

3.2 DLS

The DLS measurements were carried out by means of the instrument Zetasizer Nano ZS90 (Malvern Instruments Ltd., laser wavelength centered at 532 nm) which is able to perform size measurements in a range from 0.6 to 6000 nm. The DLS measurements were acquired while setting the detector at an angle of 173° to the laser beam axis to avoid its saturation.

In the DLS instrument, a monochromatic light beam (usually a low power cw-laser) is used to interact with a colloidal sample. When the electromagnetic waves encounter spherical particles in their pathway they absorb and further scatter the electromagnetic waves in all of the directions, consequently the scattered waves interfere with each other. As the scattered light arise from particles suspended in a liquid in a random way, the resulting interference pattern do not display a periodic behavior but rather a random one known as speckle pattern. The pattern is later captured by a light detector and transformed into a signal (Fig. 3.2). Since the particles suspended in a liquid are continuously moving due to the Brownian motion, the pattern changes through the time and so the measured intensity fluctuates. As the smaller particles move faster, the fluctuation will be also stronger. The intensity fluctuation is recorded at different time intervals and compared with each other resulting in a correlation curve that has an exponentially decreasing behavior. The rate of the exponential decay is proportional to the diffusive coefficient of the particles which is related to the particle's size through the Stokes-Einstein equation (eq. 3.7). [58]

$$D = \frac{k_b T}{6\pi\eta r} \quad (3.7)$$

where k_b represents the Boltzmann's constant, T the temperature of the medium, η the viscosity of the medium and r the size of the particles. Therefore, the bigger diffusion coefficient is, the smaller size of the particles is detected.

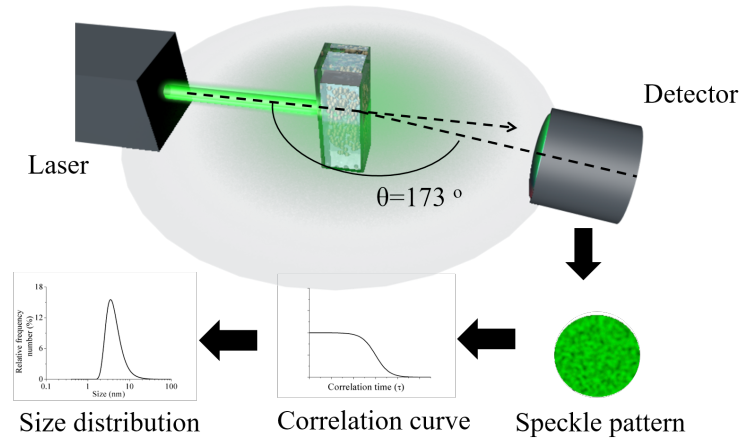


Figure 3.2: Scheme representing how the DLS instrument works.

3.3 LDV

The LDV technique is performed by means of the instrument used for the DLS measurements. The device has a pair of electrodes that enables an electrical current to pass through the colloidal sample which is used to measure the velocity of the particles while performing an electrophoresis experiment.

During the LDV experiment, a voltage is applied to the electrodes in contact with the sample. The light from the instrument interacts with the particles which surface is positively or negatively charged. As the particles are surrounded by the opposite charged ions (the particle and surrounding ions form an electrical double layer protecting the particle against interaction with other particles and thus against agglomeration), the applied voltage causes the movement of the charged carriers (particles and ions in the liquid medium) towards the opposite charged electrode and then the instrument records the velocity of the particles. Such velocity is known as the electrophoretic mobility of the particles associated to the Zeta potential through the Henry's equation (eq. 3.8). [59]

$$V_E = \frac{\epsilon z}{\eta} \quad (3.8)$$

where, V_E represents the electrophoretic mobility value, ϵ the dielectric constant of the particle, η the viscosity of the medium and z the Zeta potential.

Therefore, the Zeta potential value indicates the intensity of the static electric field of the electrical double layer at the interface between the particle and the surrounding liquid medium. In other words, if the Zeta potential is large, the particles will repel each other, i.e., avoiding an agglomeration phenomenon (Fig. 3.3).

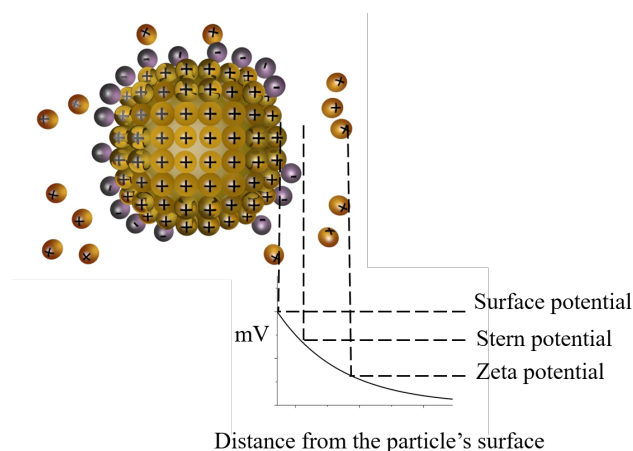


Figure 3.3: Graphical illustration of the Zeta potential.

3.4 HR-TEM

The HR-TEM micrographs from which the size, morphology and crystallographic structure of selected samples was obtained, were taken using a JEOL JEM 2100 TEM instrument that uses a bright LaB6 source operated at an acceleration voltage of 200kV.

In HR-TEM, an electronic beam is used to interact with the studied samples under vacuum conditions. The beam is further accelerated and focused by a set of strong magnets (condenser and objective lens, respectively) in the sample holder typically composed by a copper grid and a carbon film that serves to support the solid content of the samples (Fig. 3.4).

The collisions between the incoming accelerated electrons and the electrons of the sample enable their scattering and transmission through the sample. The transmitted electrons are collected by a charge-coupled-device (CCD) camera and further interpreted as an image of the specimen under study. Using the correct conditions, the HR-TEM enables to reach a resolution under 0.1 nm, making possible to determine the crystallographic structure of the samples.

The way to prepare the samples for HR-TEM inspection is the following: a droplet of the colloidal sample is poured on the sample holder and after the droplet gets dried the sample holder is introduced in the HR-TEM instrument for the corresponding inspection.

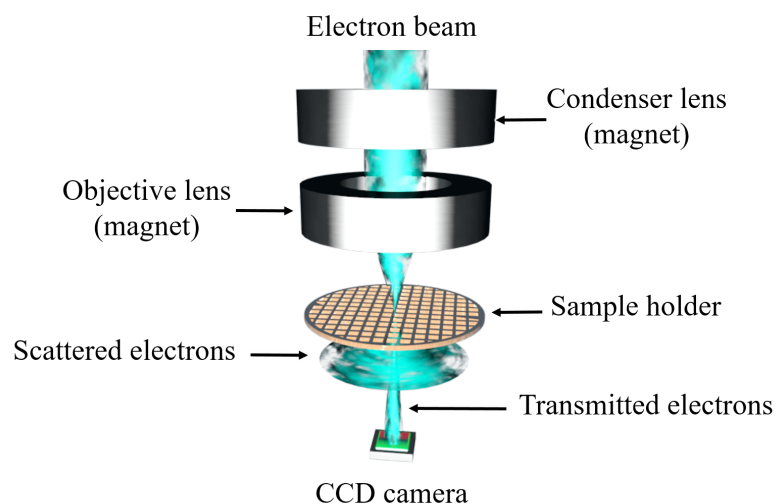


Figure 3.4: Minimal scheme of a HR-TEM instrument representing the parts described in the text.

3.5 ICP-OES

Besides the specification of the optical properties, size, shape, crystallographic structure and stability, the characterization of the sample's chemical composition is required. The chemical composition of the synthesized material is determined by means of an ICP-OES spectrometer (Perkin Elmer Optima 2100Dv) which reaches a determination of trace elements > 0.2 ppb.

The ICP-OES is a type of emission spectroscopy using an inductively coupled plasma to promote the excitation of the electrons of the higher energetic levels of different atoms. After the excitation, the electrons go back to their basal state emitting photons at a characteristic wavelength depending of the chemical element. The intensity of the corresponding emission is proportional to the number of atoms of the chemical element that is present in the studied sample.

To perform the measurements, the colloidal sample is injected to a nebulizer system that creates an aerosol with the sample. Subsequently, the aerosol is directed by an argon flowing line to an argon-based plasma which is created and stabilized by high-frequency alternative magnets. In the plasma, the sample is atomized and ionized generating the emission spectra at the characteristic wavelengths of the elements involved. Finally, an optical spectrometer allows to determine the intensity of the signal and with it the amount of material in the sample (Fig. 3.5).

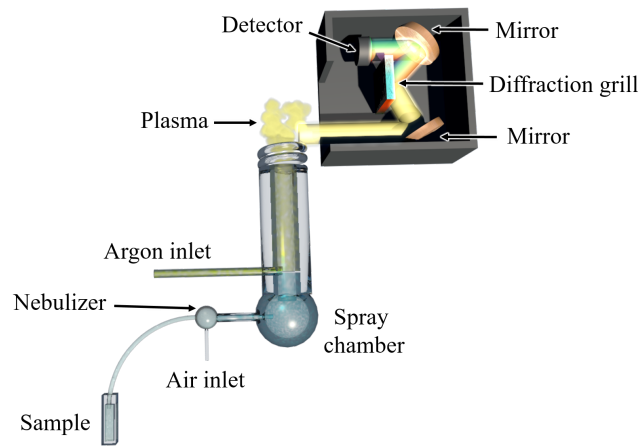


Figure 3.5: Scheme of the basic elements of an ICP-OES spectrometer.

4 Setup details

The synthesis of the Fe nanoclusters is carried out by the nanosecond laser irradiation of a colloidal solution.

The general experimental architecture is displayed in the Fig. 4.1. The main components are 3 silver-coated mirrors, three lenses, a vial that contains the colloid, a magnetic stirrer device and a Nd:YLF pulsed laser source (Litron Lasers; LDY300 PIV Series) which delivers laser radiation centered at a wavelength of 527 nm in its second harmonic generation, pulses with a time duration of 150 ns full width at half maximum (FWHM) it has two optical cavity system that enable to deliver the laser radiation at a repetition rate of 2000 Hz (1000 Hz for each optical cavity), a maximum output energy of 25 mJ and an output beam of 5 mm at width of $1/e^2$.

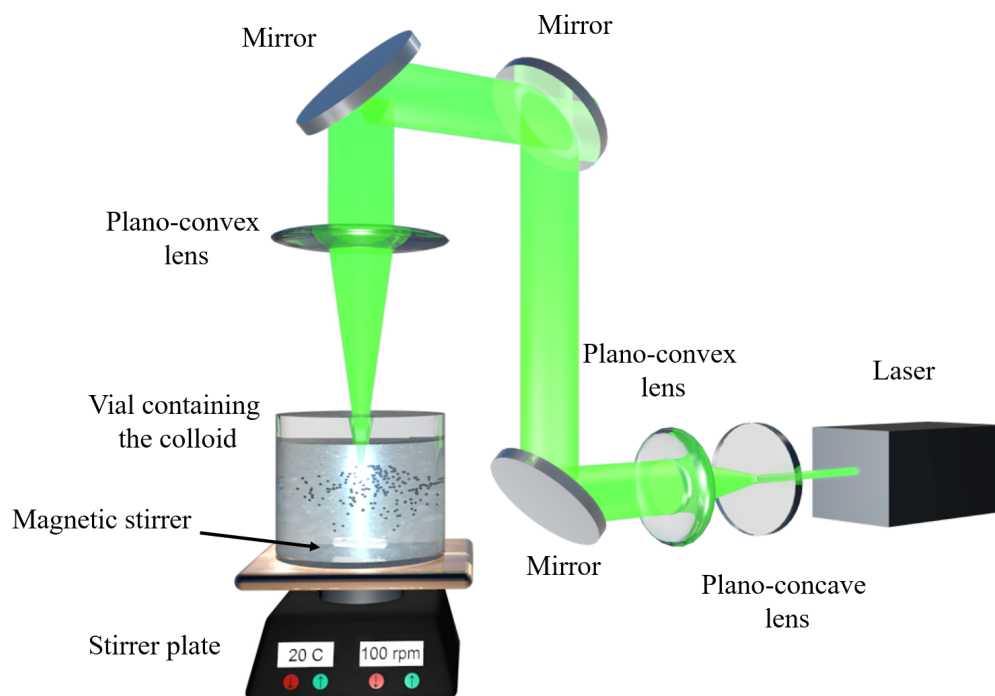


Figure 4.1: Experimental setup used for the synthesis of Fe nanoclusters with an energy fluence that exceeds the energy threshold required to evaporate the CI microparticles.

The laser beam is first expanded by a Galilean telescope consisting of one plano-

concave lens ($f = -150$ mm) and one plano-convex lens ($f = 75$ mm), giving a total magnification of 2x. The expansion of the collimated beam enables reducing the power density in the beam pathway leading to increasing the optical elements life time and decreasing the laser-mediated damage. Subsequently, the expanded beam goes through 3 mirrors which settle its direction to either the last plano-convex lens ($f = 35$ mm) used to focus the laser beam at 4 mm in-depth of the colloid, or directly to the colloid, depending on the laser fluence required for the experiment.

A teflon coated magnetic stirrer is placed inside of the colloid enabling its continuous movement due to the own rotation of the stirrer (100 rpm) caused by the magnetic field of a stirrer plate placed under the sample. The flow of the colloid allows the incoming laser beam to irradiate as many particles as possible due to their circulation.

The colloids used for the irradiation process consist of an specific solvent mixed with CI particles (HQ grade, BASF, Germany) with predominant size of 2 μm and spherical shape. The used solvents are ethanol (99.9%), water (18.2 M Ω ·cm), ethylene glycol (EG; anhydrous, 99.8%), polyethylene glycol with average mol. wt. 400 (PEG 400) and methanol (99.9%). All the mentioned polar solvents are commonly used in the synthesis of Fe NPs according to the literature. [60, 61, 62, 63, 64] In addition, as the laser-mediated reduction of the microparticles size is understood in terms of the heating-melting-evaporation theory, liquid nitrogen is tested as a possible solvent in the current thesis. The hypothesis behind the use of liquid nitrogen is that by reducing the temperature of the particles it may be possible to reach their complete evaporation in a more efficient way.

The concentrations of all colloids are 0.4 mg/mL and the volumes of the colloids are 10 mL. This concentration is chosen as the ideal possible concentration, which reflects increasing fabrication efficiency associated with increasing concentration and at the same time decreasing frequency of unwanted effects derived from a large abundance of microparticles, such as aggregation, etc. [65]

Moreover, because the first experiments for the colloid that used methanol as the solvent showed the creation of a carbon-based shell around the particles which was conventionally explained by the solvent pyrolysis derived from the high temperatures reached during the laser irradiation, [66] it became necessary the use of a capping agent to avoid the shell creation around the particles. The chosen capping agent is the sodium dithionite ($\text{Na}_2\text{S}_2\text{O}_4$), conventionally used to stabilize and modify the morphology of Fe NPs. The concentration used is 1.1 g/L, as reported in previous study. [67]

Finally, the samples are prepared in duplicate to compare the results after the laser irradiation using a laser fluence that exceeds the energy threshold required to completely evaporate the microparticles with the results obtained after using a low fluence (lower than the required energy threshold).

In this context, the first set of samples are irradiated at an average power of 10 W. The last plano-convex lens ($f = 35$ mm), third lens from the laser to vial pathway in the Fig. 4.1, enables to exceed the fluence threshold necessary to completely evaporate the microparticles for all the used solvents, as it is mentioned in the theoretical background chapter. The second set of samples are irradiated at an

average power of 700 mW. The laser beam is not focused by the third plano-convex lens in order to irradiate the samples with a lower fluence as displayed in Fig 4.2 (this setup not enable to reach the threshold energies for any solvent).

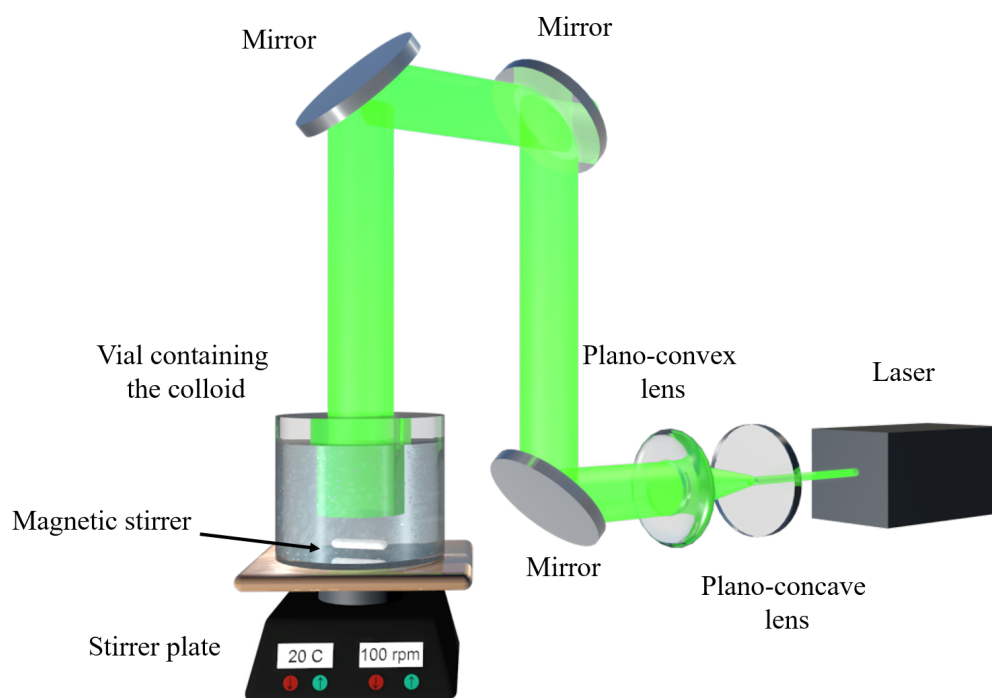


Figure 4.2: Experimental setup used for the synthesis of Fe nanoclusters with a lower energy fluence that the one required to evaporate the CI microparticles.

5 Results

5.1 Preparation and synthesis

In this thesis, different colloidal samples were subject to the previously described laser-mediated synthesis strategy. Afterwards, they were analyzed by the above explained characterization techniques. The details of the different samples under study can be found in the table 5.1.

Name of sample	Precursor	Liquid medium
S1	CI microparticles	Ethanol (C_2H_5OH)
S2	CI microparticles	Water (H_2O)
S3	CI microparticles	Ethylene glycol ($C_2H_6O_2$)
S4	CI microparticles	Polyethylene glycol 400 ($C_{2n}H_{4n+2}O_{n+1}$, $n = 8.2$ to 9.1)
S5 ¹	CI microparticles	Liquid nitrogen (N_2)
S6	CI microparticles	Methanol + Sodium dithionite ($CH_3OH + Na_2S_2O_4$)

Table 5.1: List of samples used to synthesize Fe nanoclusters

All the colloidal samples had the same before mentioned concentration (for S6, the sample in addition had a concentration of 1.1 g/L concentration of sodium dithionite) and were well mixed by a MIX ARGOLab Vortex Mixer.

Subsequently, they were irradiated by nanosecond pulsed laser radiation for a period of 30 min. The theoretical laser fluence threshold required to fully evaporate the CI microparticles is listed in the following table 5.2.

However, as expressed in the previous chapter, in order to compare two extreme situations, in the thesis we have irradiated the samples with two different fluence regimes, a lower than the one required to fully evaporate the material $4.6 \cdot 10^{-4} J/cm^2$ and one that exceeds it $4.3 \cdot 10^4 J/cm^2$. Both laser fluences were used for all the samples due to comparison purposes.

After the irradiation, the samples were centrifuged for 15 minutes at 14500 rpm (Centrifuge MiniSpin[®] plus, non-refrigerated, with Rotor F-45-12-11, 230 V/50 – 60 Hz) to separate them into a sedimented material and a transparent supernatant. Considering the size of the nanoclusters, they tend to behave like molecules and

¹ N_2 was used in the sample S5 as a solvent before their irradiation, but after the irradiation, the N_2 evaporated and the sample was transferred to C_2H_5OH for its further characterization.

Sample	Calculated $\Psi_{theoretical}$ (J/cm^2)	Calculated Ψ_{real} (J/cm^2)
S1	23.2	38.6
S2	23.2	38.0
S3	23.2	41.2
S4	23.2	48.0
S5 ²	-	-
S6	23.2	42.5

Table 5.2: List of fluence thresholds required to fully evaporate the CI microparticles. Both values obtained by means of the heating-melting-evaporation model.

therefore, only the particles with bigger sizes are sedimented during the centrifuging process. The supernatants were put in new clean vials and the sedimented materials were re-dispersed in their corresponding pure solvents. Further, they were homogenized by ultrasonic bath by means of an ultrasonic cleaner (SONOREX DIGITEC DT 510 H, 35 kHz, 9.7 L). Subsequently, each sample with the supernatant and the sediment was subject to the different characterization methods.

The hydrodynamic size measurements were taken during the 48 hours after irradiation and the Zeta potential measurements one week after the irradiation. The UV-Vis measurements were accomplished within 3 weeks. Further, the TEM and ICP-OES analysis were performed 3-4 months after the irradiation.

5.2 UV-Vis and fluorescence

The UV-Vis spectroscopy measurements were performed in a wavelength range of 250 to 800 nm at a resolution of 1 nm. First, the pure solvent was used to determine the null absorption level and subsequently the measured absorption of the sample showed the own absorption value of the Fe particles.

As displayed in various Mie Calculators, [57] for Fe 2 μm particles, no any absorption peak or valley is expected, but for particles below 20 nm an increasing absorption is expected when approaching shorter wavelengths. As displayed in the table 5.3, the experimental data obtained for the UV-Vis spectroscopy shows the expected results except for S4 which exhibits an unexpected valley (minimum of absorption value) around 255 nm even for the sample without laser treatment.

The UV-Vis spectroscopy graphs belonging to the irradiated samples showed specific curves and it is possible to observe some absorption differences in comparison with the results for the non-irradiated samples.

In the case of S1, the spectra for the sediment of both irradiated samples (below and beyond threshold) is similar as the one of the non-irradiated sample. However, for the supernatant there is a decrease in the absorption intensity and for the case of beyond threshold, an absorption peak appears in the UV region.

²The $\Psi_{theoretical}$ and Ψ_{real} values are not reported for liquid nitrogen due to the lack of information about its enthalpies and the issues related to their measurement.

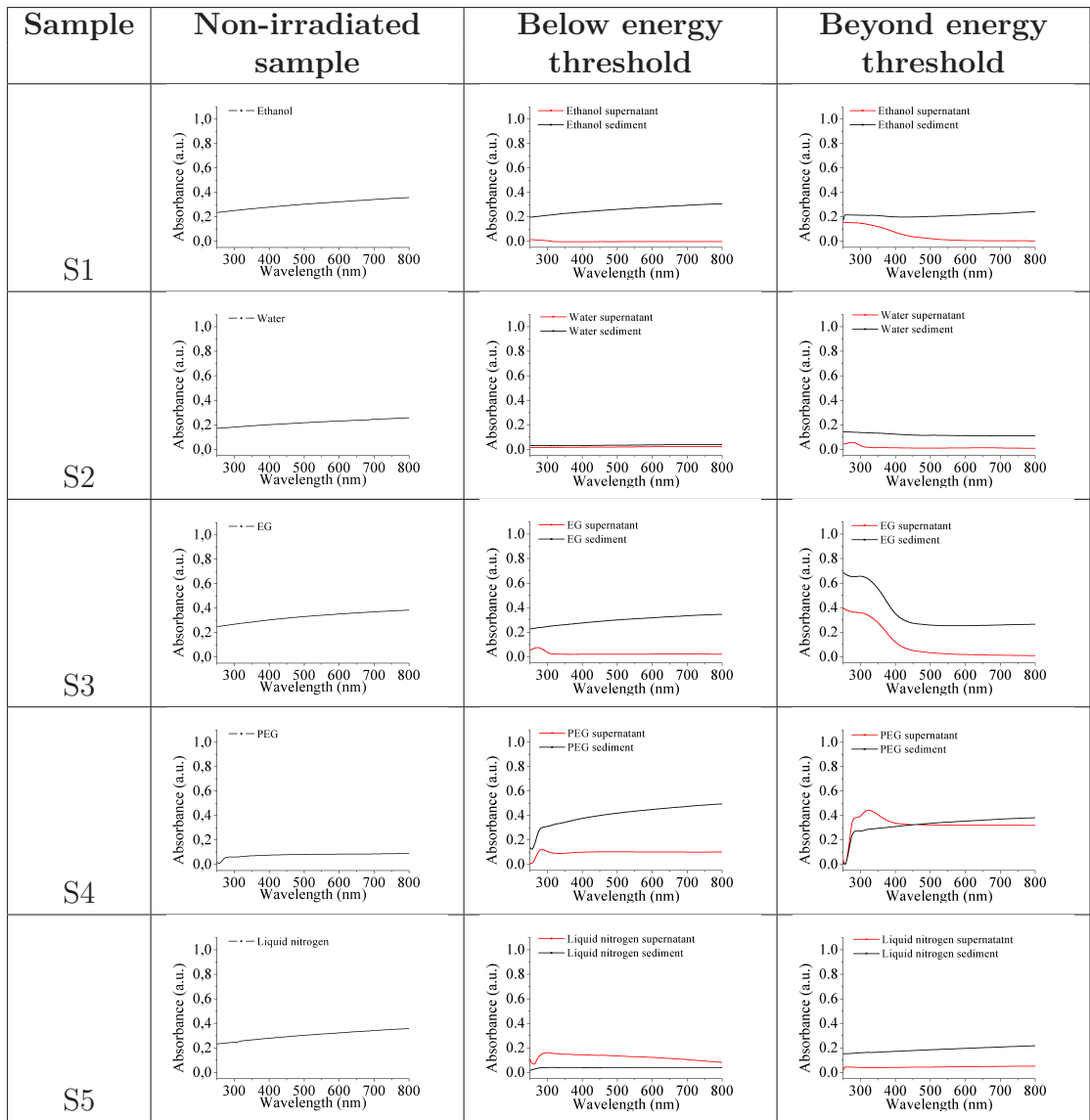


Table 5.3: List of UV-Vis spectra of the samples before the laser irradiation (Non-irradiated sample), after laser irradiation using a fluence value lower than the threshold value required to fully evaporate the microparticles (Below energy threshold) and after laser irradiation using the high fluence value (Beyond energy threshold). In addition, the graphs corresponding to the irradiated material include the spectra of the supernatant and the sediment.

In the case of S2, the most notable difference between the non-irradiated and the irradiated samples is a reduction in the absorbance intensity and aside of that, the supernatant of the beyond energy threshold shows again a peak in the UV region, to be more specific at 275 nm.

In the case of S3, the supernatant of the below energy threshold shows a peak around 272 nm and both, the supernatant and the sediment of the beyond energy threshold exhibit a peak at 310 nm and 300 nm, respectively.

For S4, the sample without laser irradiation shows a valley at 255 nm. The same valley is preserved for the irradiated samples. However, for the supernatant of both, below and beyond energy threshold, an absorption peaks appears at 284 nm. In addition, a further peak appears for the beyond energy threshold supernatant at 323 nm.

For S5, the below threshold supernatant exhibits a valley at 258 nm. Finally, the UV-Vis analysis was not performed for S6 because the addition of $Na_2S_2O_4$ makes impossible to correctly compare the curves with any available theoretical model.

In addition, the significant valley followed by a couple of peaks found for the the beyond energy threshold supernatant of S4 leads to the suspicion of a possible interesting optical property. For this reason, it was decided to measure the fluorescence of the colloid by means of a Spark 10 M multimode microplate reader (TECAN), the excitation wavelengths were selected to be in the range of 240 to 300 nm with an excitation step size of 10 nm, the emission wavelength range was taken from 320 to 800 nm with a step size of 10 nm.

Essentially, the instrument is used to irradiate the colloidal sample with an specific wavelength. After filtering the excitation wavelength, the potential emission of light coming from the sample detect.

The fluorescence spectrum displayed in Fig. 5.1 shows a significant emission of light at the wavelength of 440 nm while the colloid is excited at the wavelength of 260 nm.

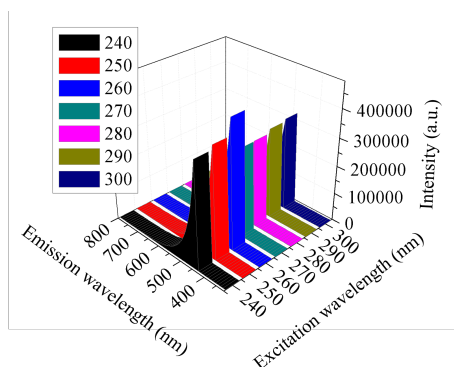


Figure 5.1: Fluorescence spectra of S4.

5.3 DLS

The table 5.4 displays the hydrodynamic size distribution of the samples measured by the DLS technique. Moreover, the table 5.5 presents the maximum value and the width of the corresponding size distributions. From the graphs, it is possible to observe that the hydrodynamic size of the non-irradiated samples is almost the same for all the liquids. However, after the laser irradiation either using a fluence lower than the energy threshold or a higher one, both the sediment and the supernatant experience a change.

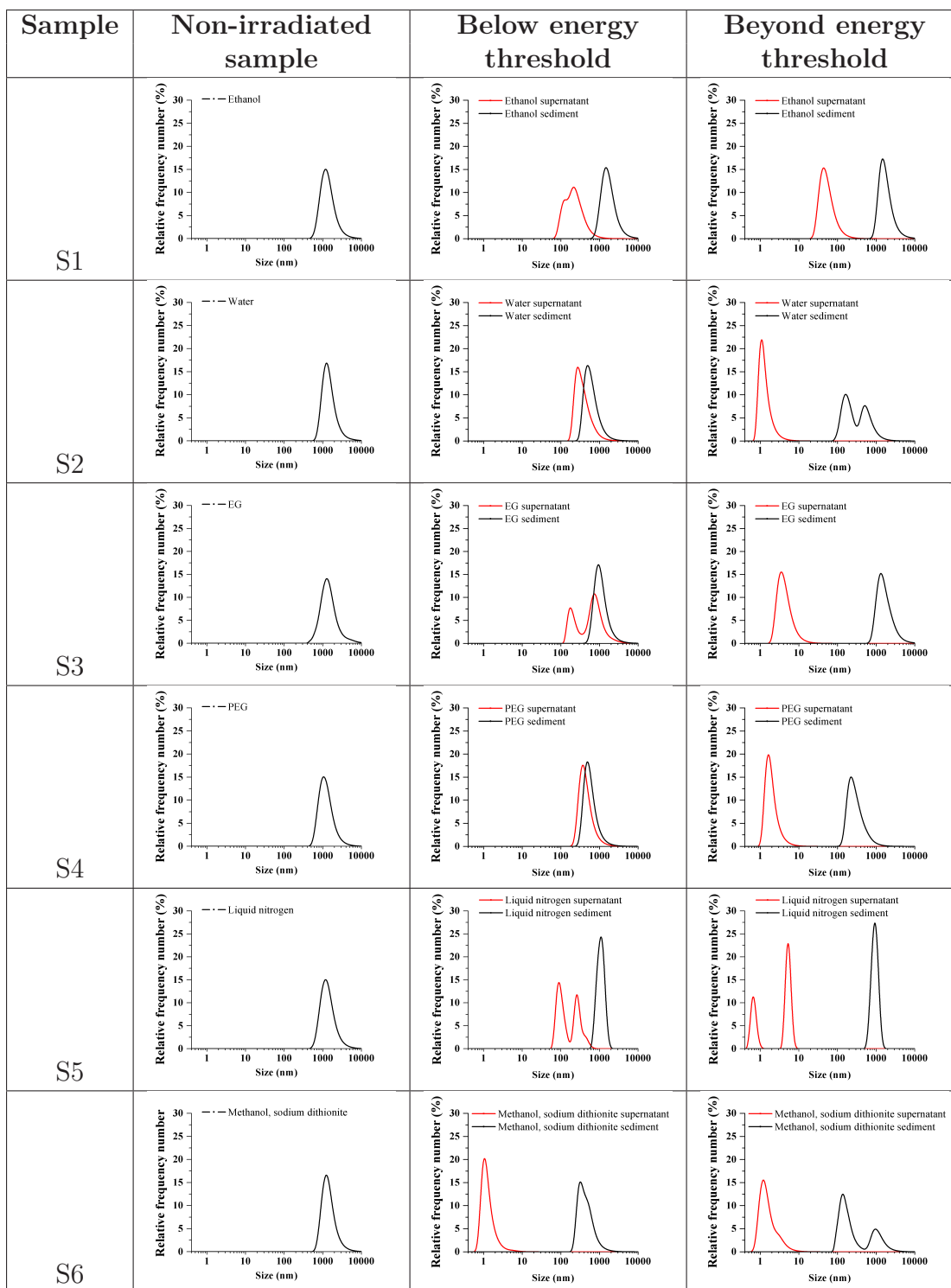


Table 5.4: List of DLS graphics.

For S1, only the sediment of both, the sample irradiated with a low laser fluence and a high one, exhibits an important decrease in the hydrodynamic size. In the case of S2, the most significant change is observed when the sample is irradiated

with a higher laser fluence than the one required to fully evaporate the precursor particles. In this situation, the hydrodynamic size indicates that we are already obtaining the Fe nanoclusters.

Similar to the S2, for S3 the most important change is observed while using the high laser fluence. Even when the hydrodynamic size do not correspond to the range of sizes of the Fe nanoclusters, it is possible to observe a hydrodynamic size distribution smaller than 10 nm. For S4, as in the previous 2 cases, while irradiating the sample with the high laser fluence it is possible to get a considerable size reduction. However, for this sample it is possible to get the size values associated to those of Fe nanoclusters.

Analogous to S2, S3 and S4, for S5 the size distribution that corresponds to the Fe nanoclusters is observed while using the high laser fluence. Finally, in the case of S6, it is possible to observe the size of the Fe nanoclusters for both irradiation regimes.

Sample	Hydrodynamic size (nm)									
	Non-irradiated sample		Below energy threshold				Beyond energy threshold			
	Bulk		Supernatant		Sediment		Supernatant		Sediment	
	M	W	M	W	M	W	M	W	M	W
S1	1176.4	1107.1	1475.8	1369.7	216.7 and 126.4	248.4 and 108.6	1473.8	1217.3	43.7	42.0
S2	1255.2	1027.0	493.5	447.2	274.6	269.7	511.4 and 162.4	437.3 and 138.2	1.1	0.6
S3	1266.0	1200.1	941.7	765.6	740.2 and 176.2	607.6 and 109.8	1328.0	1314.2	3.5	3.3
S4	1047.7	1001.5	486.6	374.1	370.3	300.2	224.1	226.6	1.6	1.1
S5	1176.4	1107.1	1095.6	633.4	260.1 and 89.0	118.0 and 50.6	925.2	482.6	5.3 and 0.7	2.2 and 0.3
S6	1234.6	1033.2	319.3	377.0	1.1	0.7	964.0 and 137.5	840.4 and 111.6	1.2	1.0

Table 5.5: List of hydrodynamic sizes, where M means maximum value of the size distribution and W refers to its width.

5.4 LDV

The table 5.6 shows the Zeta potential values of the samples before and after the laser irradiation. The measurements were taken after one week of the synthesis to ensure that the values which are related to the stability of the colloid were reliable towards the use of the nanomaterial after a period of one week of storage.

Before the laser irradiation, the most of the samples seem to have a Zeta potential value beyond $|30mV|$ which indicates a long-term stability. Moreover, the sample S6 exhibits excellent stability.

After the laser irradiation, the only samples that exhibit a Zeta potential value beyond or close to $|30mV|$ are S3, S4 and S6. Therefore, the rest of the samples seem to have a poor stability through the time.

Sample	Zeta potential (mV)				
	Non-irradiated sample	Below energy threshold		Beyond energy threshold	
		Supernatant	Sediment	Supernatant	Sediment
S1	39.0	2.7	18.3	8.7	7.6
S2	34.9	0.0	11.4	0.0	6.4
S3	42.9	28.4	30.4	33.6	28.8
S4	133.0	116.0	75.5	110.0	56.1
S5	39.0	1.9	5.9	0.0	6.3
S6	15.1	17.3	38.6	14.4	42.9

Table 5.6: Zeta potential values

5.5 HR-TEM

The table 5.7 displays a list of 3 micrographs for the supernatant of each sample irradiated with a fluence beyond threshold. One general micrograph with a scale bar of 10 μm , one micrograph with a middle scale bar of 0.1 μm and one micrograph at a high resolution with a scale bar of 10 nm. The micrographs were used for the determination of the real size of the synthesized particles. In the program ImageJ, 200 particles for each supernatant were measured and the corresponding size histograms were created.

In general, it is possible to observe Fe nanoclusters in the majority of the samples, except for the samples S1 and S5. In the case of S1, it is possible to observe that after the 3-4 months, which as previously mentioned is the time in between the synthesis of the samples and the HR-TEM measurements, the synthesized NPs could create a layer of oxide that eventually became a dendrimer-like structure that connected the Fe NPs. As it is appreciated in the micrograph with the scale bar of 10 nm, apparently there are some NPs trapped in the oxide structure. In fact, the size histogram was estimated considering only the size of those NPs.

For S5, the particles seem to form big assemblages and the histogram reflects the size of the individual Fe NPs forming the assembles.

In addition, in the general micrograph (10 μm) of S4 it seems that there are some concentric circles. To perform the HR-TEM measurements it is mandatory to dry the solvent from the samples. However, in the case of S4 where the solvent is PEG 400 the sample was not completely dried up, due to the high boiling point of PEG 400 and thus, a thin film of PEG 400 still remained in the sample holder. Therefore, when the electron beam was highly focused in the sample for long periods of time, it burned up the PEG 400.

Finally, a HR-TEM micrograph is included (Fig. 5.2) to show the potential crystallographic families of the synthesized particles. The micrograph shows a representative image of the supernatant of S3 after undergoing a high laser fluence

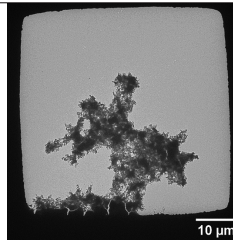
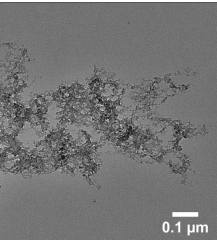
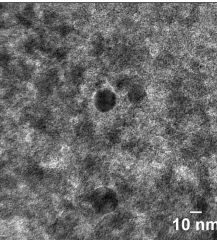
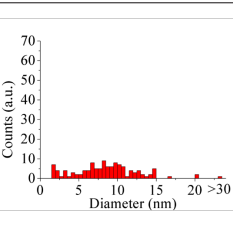
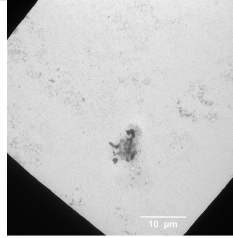
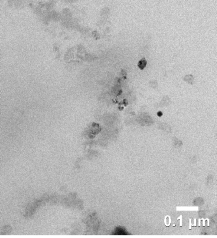
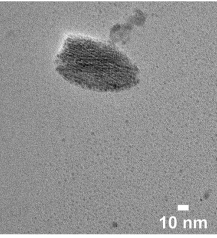
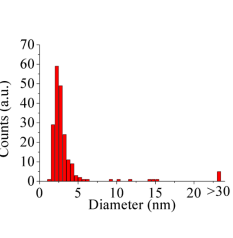
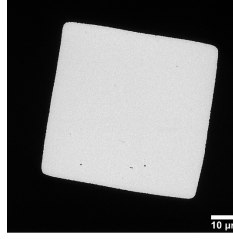
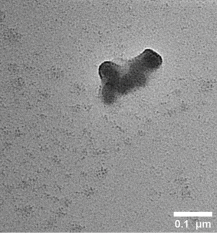
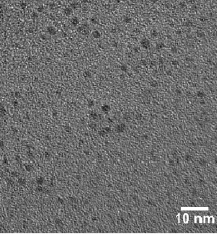
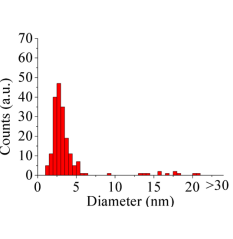
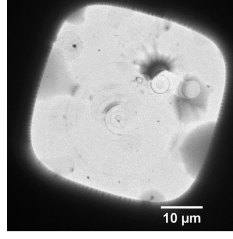
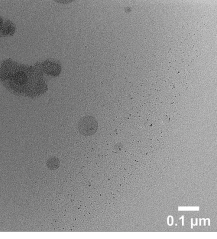
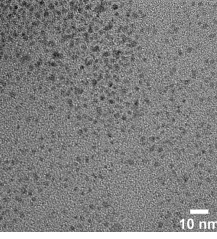
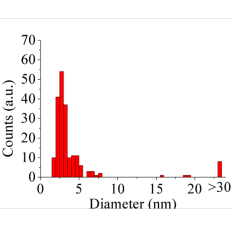
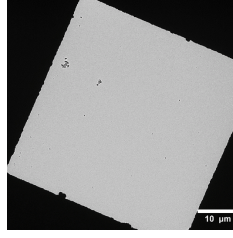
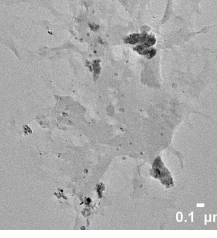
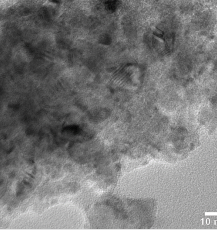
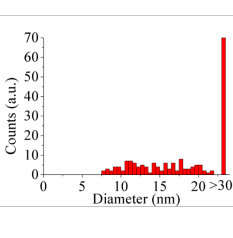
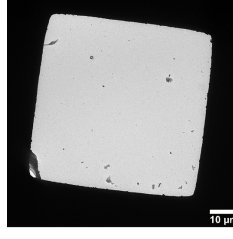
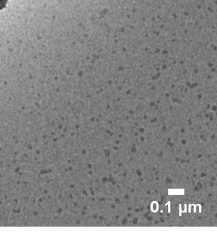
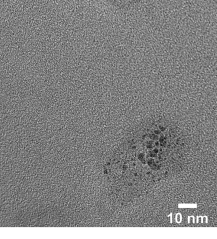
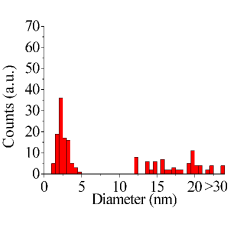
Sample	TEM images and size histograms			
S1				
S2				
S3				
S4				
S5				
S6				

Table 5.7: List of TEM images and size histograms of the supernatant of the corresponding samples irradiated at a high laser fluence.

irradiation. The measured interplanar distances are 1.97 ± 0.13 Å and 3.37 ± 0.17 Å. According to the JCPDS databases, the crystallographic families could belong to $\epsilon - Fe_2O_3$ (PDF: 16-653) of a monoclinic crystal system with molecular formula per unit cell ($Z = 20$) associated to the $(-4\ 4\ 1)$ and $(2\ 0\ 2)$ planes, respectively.

This is the only sample that exhibited consistent crystallographic families for a large number of particles. This is the reason why it is the only sample used for the crystallographic analysis.

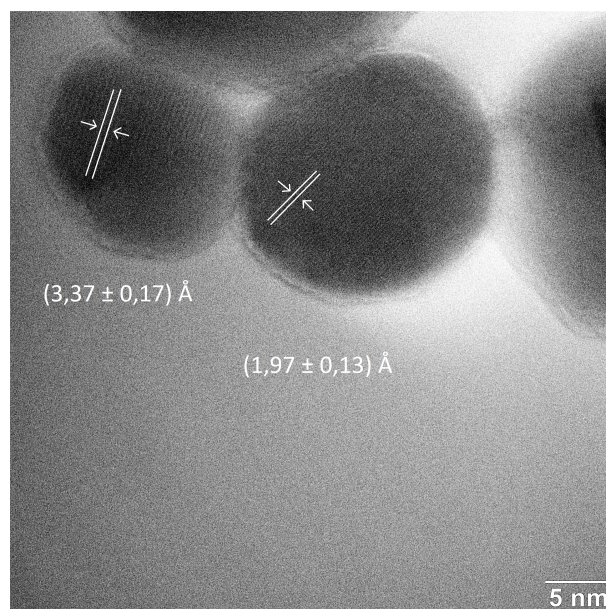


Figure 5.2: HR-TEM micrograph of sample S3 where it is possible to observe its crystalline nature.

5.6 ICP-OES

Another significant technique was ICP-OES and it was used to determine the iron concentration in the colloids. The results are summarized in the table 5.8 and together with the calculated median diameter of the particles obtained from the histograms it was possible to calculate the number of particles in 1 mL of each corresponding colloid and to calculate their effective surfaces.

In addition, it is important to mention that the sample S6 is not reported due to its confusing values. However, future experiments are planned in order to understand the issues related to its measurements by means of ICP-OES.

Sample	Concentration of Fe (mg/L)			
	Below energy threshold		Beyond energy threshold	
	Supernatant	Sediment	Supernatant	Sediment
S1	< 0.02	46.70	6.35	71.70
S2	0.61	1.29	< 0.02	2.41
S3	0.02	35.50	2.47	212.00
S4	< 0.02	105.00	1.19	149.00
S5	< 0.02	210.00	< 0.02	213.00
S6	-	-	-	-

Table 5.8: Concentration of Fe measured by ICP-OES.

6 Discussion

In general, the collected results provide an important insight into the optical, morphological, stability and structural properties of the synthesized nanomaterials, enabling to understand the conditions required to synthesize Fe nanoclusters.

For example, the UV-Vis spectroscopy measurements allowed to understand that when the CI microparticles were dispersed in all the different liquid mediums, the only remarkable behavior was that the absorption intensity gets equally incremented for all the wavelengths in the spectrum from 250 - 800 nm, except for the case of S4 which displayed a valley around 255 nm. When comparing with the Mie calculators, [57] the theoretical absorption spectra coincides with the results. Moreover, in all of the cases, when the laser fluence used to irradiate the samples is way below the fluence threshold required to fully evaporate the CI microparticles, there are not significant changes. The sediment of such samples exhibits a similar absorption intensity as in the case of the non-irradiated samples and the supernatant shows the corresponding absorption intensity.

The only interesting behavior is observed for the samples S3, S4 and S5 where a small peak seems to appear around 280 nm for S3 and S4 and a valley appears around 250 nm for S5. When comparing with the Mie calculators, such peak only appears when the size of the Fe NPs is lower than 20 nm while dispersed in a wide variety of solvents. Therefore, it is possible to infer that after the centrifuge process NPs with sizes below 20 nm could be dispersed in the supernatants of samples S3 and S4 when the sample was irradiated at a low laser fluence. In the case of S5 it was not possible to determine any reason behind the existence of the valley, however, after comparison with S4 it is believed that a crossed contamination could take place. Nevertheless, after repeating several times the measurement, while cleaning in a deep way all the experimental equipment, the behavior didn't change, therefore, it is considered that this anomaly require a further study which is out of the scope of the thesis.

When the samples were subject to a high laser fluence, the sediment again did not show any significant change in comparison with the non-irradiated samples, except for the case of S3, which exhibited an absorption peak at around 300 nm and also a high absorption intensity for the rest of the wavelengths. After the comparison with the Mie calculators, this characteristic peak appears when Fe NPs with a size of 50 nm are dispersed in a wide variety of solvents. Therefore, it is feasible that a combination of agglomerated small particles and big particles in the sediment of S3 resulted in the observed absorption spectrum. In the case of the supernatant, all of the samples (except S5) showed a peak at short wavelengths which according to

the theory belongs to Fe NPs with sizes below 20 nm. Moreover, S3 and S4 exhibited the peak around 310 nm which according to the theory belongs to NPs with a size of 50 nm. Therefore, from this results is possible to say that the irradiation of the samples with a high laser fluence led to the reduction of the CI microparticles.

In addition, a complementary fluorescence test was performed for the supernatant of the sample S4 after the high laser fluence irradiation as the sample exhibited the largest difference between its absorption valley and peak. Such difference has been previously observed in materials that exhibit fluorescence emission when they are in contact with PEG 400. [68] For our case, the sample exhibited a light emission in 440 nm while using 260 nm as the wavelength or excitation. As described in different reports, the combination of metal NPs and poly(ethylene glycol) species with different molecular weights leads to the observation of fluorescence emission due to such macromolecules have double-ended groups with a strong dipole moment serving to attach to the metal NPs surface. Thus the surface of the capped NPs may present electron-dense regions that lead to the fluorescence emission. [69]

Therefore, our observation may serve as a seminal study for the further exploration of fluorescence emission while using poly(ethylene glycol) species to stabilize metal NPs.

Aside of the UV-Vis spectroscopy and fluorescence analyses, the DLS technique allowed to observe that the mean hydrodynamic size values of the CI microparticles were in all of the solvents larger than 1 μm , corresponding to the real size from the material's datasheet. Nevertheless, the irradiation caused its size reduction which can be confirmed from the supernatant measurements, especially for those irradiated with a high laser fluence. Whereas, the sediment material size was similar to the non-irradiated material or was not significantly reduced. This result can be caused by a lack of irradiation of all of the particles in the colloids or by the irradiation of the particles away from the focal point of laser beam which could match the energy threshold required for a full melting but not for a full evaporation, previously as suggested by different research groups. [54, 70]

The irradiation with laser fluences beyond the energy threshold required to fully evaporate CI microparticles allowed the generation of nanostructures which hydrodynamic size distributions were in the size regimen of the nanoclusters except for the sample S1. Considering that in the current experiment it was used laser fluences that were 3 orders of magnitude larger than the full evaporation threshold, it is believed that we should generate nanoclusters for all of the samples and therefore, the not successful observation of such small particles can be due to insufficient sensitivity of the DLS instrument in detecting the scattered light intensity of ultra-small nanoparticles or due to a low stability of the particles. This claim can be confirmed by the Zeta potential measurements which were really low for S1 after the laser irradiation. The correct interpretation of the Zeta potential values is performed according to the table 6.1, which content can be found elsewhere. [71, 72, 73]

For S1, the Zeta potential measurements reveal that after the laser irradiation, either at low or high laser fluences, the sample became unstable, the same happened with S2 and S5. Notwithstanding, the Zeta potential values verify a relatively good stability for S3 and an extraordinary stability for S4. The reason behind this can

Zeta potential (mV)	Stability behavior of the colloid	
From 0 to 5	Not stable	Rapid coagulation or flocculation
Beyond 5 to 10		Intermediate zone
Beyond 10 to 30		Incipient stability
Beyond 30 to 40	Stable	Moderate stability
Beyond 40 to 60		Good stability
Beyond 60		Excellent stability

Table 6.1: Colloidal behavior according to the Zeta potential values.

be connected with the structure and dipole moment of EG (S3) and PEG 400 (S4). The capping effect as well as stability of the particles is proportional to the dipole moment of the solvents, which are 1.69 D, 1.85 D, 2.75 D, 3.70 D and 1.69 D for ethanol, water, EG, PEG 400 and methanol, respectively. [74, 75, 76, 77]

In the case of EG and PEG 400, their dipole moment is large in comparison with the rest of the solvents and most probably this was the reason why they acted as more efficient capping agents that enable the long-term stability of the colloids. The capping effect consists in the attachment of macromolecules to the surface of the NPs surface. The molecules that have a strong dipole moment are physically adsorbed to the surface of the bare NPs and the molecules further prevent the interaction between NPs and thus, their agglomeration. [78] Moreover, as it has been previously suggested by different research groups, the PEG 400 can act as a network to capture the recently created nanoclusters due to its long molecular structure. [65] Finally, in the case of sample S6, the $Na_2S_2O_4$ was used as stabilizing agent, however, as exhibited in the table 5.6 the stability of the supernatant was not effective enough to use the material in a real application.

In addition, towards complementing the size morphology analysis of the samples, the HR-TEM micrographs were used to disclose the real size of the Fe nanoclusters. In this context, as the supernatant of the samples irradiated at a high laser fluence exhibited their presence, such samples were used for the analysis. The histograms of sizes from the corresponding micrographs ratify the predominantly presence of ultra-small nanoparticles.

Even though the histograms show the presence of Fe nanoclusters for S2 and S6, the real interpretation is more complex. In the micrographs, it is possible to see large amounts of mass including the ultra-small particles. This situation can be connected to the oxidation of material in the case of the sample with water due to autoprotolysis of water [79] and to the pyrolysis in the case of the sample with methanol. [66] Moreover, unusual structures (“dendrimers outward”) were observed for the samples S1 and S5. In the case of S1, it could be connected with the pyrolysis effect or iron oxide formation. In case of S5, the specific structures indicate a different behaviour, such as very fast cooling during the laser irradiation due to the cryogenic temperature of the liquid nitrogen (below 77 K). For this reason, the generated small particles cannot be released into the surrounding solvent and rather create

aggregates of Fe nanoclusters.

To deeply understand both, the size and stability of the synthesized Fe nanoclusters, it is necessary to take a look on the physical phenomena that can take place during the irradiation with a high laser fluence. As it was previously discussed in the first chapter, while using a ns pulsed laser source, after the incoming radiation is absorbed by the particles, they get evaporated and transfer sufficient energy to their surrounding medium, promoting the creation of a cavitation bubble that surrounds them. The bubble is composed by the molecules of the medium that turned from the liquid to the gas state. During the lifetime of the cavitation bubble, the hot species from the bubble interact with the newly created Fe nanoclusters and it is at this time where the first size quenching and stabilization process can take place, as reported just few weeks ago by Letzel et. al. [43] For the case of S1, S2, S3 and S6, it is possible to dissociate the ethanol, water, EG and methanol molecules while irradiating at the laser fluence regime that we are doing, [80] therefore, it is probable that OH^- groups promote the size quenching and stabilization of the Fe nanoclusters. Moreover, as EG also has a strong dipole moment and can act as a capping agent, a further stabilization step may take after the collapse of the cavitation bubble. In the case of S4, as PEG 400 is a macromolecule, the size quenching and stabilization may rather take place after the collapse of the cavitation bubble, when the Fe nanoclusters are released to the surrounding medium. [43]

In the case of S5, when the samples are transferred to ethanol after the complete evaporation of the liquid nitrogen, the stability of the sample can only take place due to the formation of an electrical double layer around the particles because no any other external stabilization agent is added. Finally, for S6 the particles can be stabilized through the physisorption of $\text{Na}_2\text{S}_2\text{O}_4$ to the Fe nanoclusters.

Last but not least, the ICP-OES results reveal that there is still plenty of room to optimize the technique towards getting better production rate of Fe nanoclusters. However, some interesting facts can be extracted out of it.

Considering that after high laser fluence irradiation, the final size distribution of the Fe nanoclusters was around 1.5 nm for the supernatant of the samples S3 and S4, and in combination with the ICP-OES results, it is possible to estimate that the number of synthesized nanoclusters is in the order of 10^{13} particles per mL and with this, a total useful surface of around 10 cm^2 per mL. In comparison with the same concentration of particles but with sizes of around 20 nm (i.e. a frequent Fe NPs size for catalysis applications [81]), the total useful surface per mL is one order of magnitude larger.

The rest of the samples had a very low amount of Fe mass, except for ethanol. However, it contained several times larger particles than the ultra-small particles.

To conclude, the HR-TEM micrographs show that after undergoing the high laser fluence irradiation, the S3 sample exhibited a crystallographic structure that match with the one of $\epsilon - \text{Fe}_2\text{O}_3$, which aside of the magnetic properties, shows interesting photochemical properties widely used in photocatalysis among other applications. [82]

Therefore, the findings exposed in the current thesis could have interesting implications in different nanotechnology-related fields.

7 Conclusion

In summary, the thesis deals with the production of Fe nanoclusters by means of a laser-mediated synthesis strategy known as “laser synthesis of colloids”. This strategy represents a set of low-waste producing synthesis alternatives with a lot of advantages in comparison with the conventional techniques used for the fabrication of nanoclusters, such as thermal decomposition, controlled chemical coprecipitation, microemulsion synthesis method and chemical vapor condensation. In particular, the methodology described in the current thesis is “laser fragmentation in liquids” which enables the evaporation of precursor micro or submicrometric particles to turn them into nanoparticles with ultra-small sizes. The production of such materials is important because they exhibit outstanding properties resulting from, among other characteristics, an extremely high SA:V ratio. In the view of getting the smallest possible particle size, the thesis contains well described theoretical formulas that are based on the heating-melting-evaporation model, needed to estimate the laser energy required to fully evaporate the precursor micro or submicrometric particles.

The experimental part includes the measured characteristics of Fe particles, synthesized by means of the laser irradiation of Fe-based colloids in six different solvents (ethanol, water, EG, PEG 400, liquid nitrogen and methanol). The used laser source is a nanosecond pulsed laser and the laser irradiation encompasses two different energetic levels, one below the threshold required to fully evaporate the precursor (CI particles with a size of 2 μm) and one below the threshold. In the thesis, it is possible to compare different physico-chemical characteristics of the colloidal samples before and after the laser irradiation (below and beyond energy threshold).

The techniques used to analyse the samples are the following: UV-Vis spectroscopy, DLS, LDV, HR-TEM and ICP-OES. These techniques enable to determine the absorption in UV-Vis spectra, hydrodynamic size distribution, Zeta potential, size, morphology, crystallographic structure and mass. Moreover, the fluorescence spectroscopy technique is used to assess the fluorescence emission of a selected sample. The different analyses demonstrate that it is possible to successfully synthesize Fe nanoclusters while irradiating with a beyond threshold laser fluence, colloids composed by CI particles and water, EG, PEG 400 and methanol.

In contrast, the samples using ethanol and liquid nitrogen, lead to the synthesis of bigger unwanted nanostructures, like iron oxide, carbon-shell structures and aggregates of nanoclusters.

The Fe nanoclusters exhibit a strong stability when using the solvents EG and PEG 400. According to the latest literature, this is because both solvents act as size quenching and capping agents. Moreover, the use of such solvents enables to get the

largest production rate in comparison with the rest of the solvents; $\sim 10^{13}$ particles per mL and thus, a useful surface of $\sim 10\text{cm}^2$ per mL. In addition, the use of EG leads to the synthesis of Fe nanoclusters with a crystallographic structure that matches the one of $\epsilon - \text{Fe}_2\text{O}_3$, a material extensively exploited in a wide variety of application, and the use of PEG 400 leads to the synthesis of Fe nanoclusters that exhibit fluorescence emission.

For this reason, the future prospect of the research work will be focused on the optimization of the synthesis process and the implementation of the product in real applications such as improvement of smart fluids (magnetorheological fluids and ferrofluids) for medical (e.g. MRI), technological (e.g. damping and sealing systems) and material science utilization, in the field of fluorescent biomarkers and in the field of catalysis.

References

- [1] PARR, Douglas. Nanoscience debate. *The Lancet*. 2003, vol. 362, no. 9392, pp. 1332–1333. Available from DOI: [10.1016/S0140-6736\(03\)14600-4](https://doi.org/10.1016/S0140-6736(03)14600-4).
- [2] ODOM, Teri W.; PILENI, Marie-Paule. Nanoscience. *Accounts of Chemical Research*. 2008, vol. 41, no. 12, pp. 1565–1565. Available from DOI: [10.1021/ar800253n](https://doi.org/10.1021/ar800253n).
- [3] JIN, Rongchao; ZENG, Chenjie; ZHOU, Meng; CHEN, Yuxiang. Atomically precise colloidal metal nanoclusters and nanoparticles: fundamentals and opportunities. *Chemical Society Reviews*. 2016, vol. 116, no. 18, pp. 10346–10413. Available from DOI: [10.1021/acs.chemrev.5b00703](https://doi.org/10.1021/acs.chemrev.5b00703).
- [4] KUNWAR, Puskal; HASSINEN, Jukka; BAUTISTA, Godofredo; RAS, Robin HA; TOIVONEN, Juha. Sub-micron scale patterning of fluorescent silver nanoclusters using low-power laser. *Scientific Reports*. 2016, vol. 6, pp. 23998. Available from DOI: [10.1038/srep23998](https://doi.org/10.1038/srep23998).
- [5] WILCOXON, JP; ABRAMS, BL. Synthesis, structure and properties of metal nanoclusters. *Chemical Society Reviews*. 2006, vol. 35, no. 11, pp. 1162–1194. Available from DOI: [10.1039/B517312B](https://doi.org/10.1039/B517312B).
- [6] AUFFAN, Mélanie; ROSE, Jerome; BOTTERO, Jean-Yves; LOWRY, Gregory V; JOLIVET, Jean-Pierre; WIESNER, Mark R. Towards a definition of inorganic nanoparticles from an environmental, health and safety perspective. *Nature Nanotechnology*. 2009, vol. 4, no. 10, pp. 634. Available from DOI: [10.1038/nnano.2009.242](https://doi.org/10.1038/nnano.2009.242).
- [7] DÍEZ, Isabel; RAS, Robin HA. Fluorescent silver nanoclusters. *Nanoscale*. 2011, vol. 3, no. 5, pp. 1963–1970. Available from DOI: [10.1039/C1NR00006C](https://doi.org/10.1039/C1NR00006C).
- [8] MOTTET, C; ROSSI, G; BALETTO, F; FERRANDO, R. Single impurity effect on the melting of nanoclusters. *Physical Review Letters*. 2005, vol. 95, no. 3, pp. 035501. Available from DOI: [10.1103/PhysRevLett.95.035501](https://doi.org/10.1103/PhysRevLett.95.035501).
- [9] BALETTO, F; MOTTET, C; FERRANDO, R. Reentrant morphology transition in the growth of free silver nanoclusters. *Physical Review Letters*. 2000, vol. 84, no. 24, pp. 5544. Available from DOI: [10.1103/PhysRevLett.84.5544](https://doi.org/10.1103/PhysRevLett.84.5544).
- [10] CASTLEMAN, AW; JENA, Puru. Clusters: A bridge between disciplines. *Proceedings of the National Academy of Sciences*. 2006, vol. 103, no. 28, pp. 10552–10553. Available from DOI: [10.1073/pnas.0601783103](https://doi.org/10.1073/pnas.0601783103).

- [11] ALIVISATOS, A Paul. Semiconductor clusters, nanocrystals, and quantum dots. *Science*. 1996, vol. 271, no. 5251, pp. 933–937. Available from DOI: [10.1126/science.271.5251.933](https://doi.org/10.1126/science.271.5251.933).
- [12] KONG, Yifei; CHEN, Jun; GAO, Feng; BRYDSON, Rik; JOHNSON, Benjamin; HEATH, George; ZHANG, Yue; WU, Lin; ZHOU, Dejian. Near-infrared fluorescent ribonuclease-A-encapsulated gold nanoclusters: preparation, characterization, cancer targeting and imaging. *Nanoscale*. 2013, vol. 5, no. 3, pp. 1009–1017. Available from DOI: [10.1039/C2NR32760K](https://doi.org/10.1039/C2NR32760K).
- [13] DE, Goutam et al. Metal nanoclusters: new fluorescent probes for sensors and bioimaging. *Journal of applied physics*. 2014, vol. 9, no. 1, pp. 132–157. Available from DOI: [10.1016/j.nantod.2014.02.010](https://doi.org/10.1016/j.nantod.2014.02.010).
- [14] HÄKKINEN, Hannu. Electronic shell structures in bare and protected metal nanoclusters. *Advances in Physics: X*. 2016, vol. 1, no. 3, pp. 467–491. Available from DOI: [10.1080/23746149.2016.1219234](https://doi.org/10.1080/23746149.2016.1219234).
- [15] AIKEN III, John D; FINKE, Richard G. A review of modern transition-metal nanoclusters: their synthesis, characterization, and applications in catalysis. *Journal of Molecular Catalysis A: Chemical*. 1999, vol. 145, no. 1-2, pp. 1–44. Available from DOI: [10.1016/S1381-1169\(99\)00098-9](https://doi.org/10.1016/S1381-1169(99)00098-9).
- [16] KIM, Byung Hyo et al. Large-scale synthesis of uniform and extremely small-sized iron oxide nanoparticles for high-resolution T1 magnetic resonance imaging contrast agents. *Journal of the American Chemical Society*. 2011, vol. 133, no. 32, pp. 12624–12631. Available from DOI: [10.1021/ja203340u](https://doi.org/10.1021/ja203340u).
- [17] QIAN, Huifeng; ZHU, Manzhou; WU, Zhikun; JIN, Rongchao. Quantum sized gold nanoclusters with atomic precision. *Accounts of Chemical Research*. 2012, vol. 45, no. 9, pp. 1470–1479. Available from DOI: [10.1021/ar200331z](https://doi.org/10.1021/ar200331z).
- [18] SHANG, Li; DONG, Shaojun; NIENHAUS, G Ulrich. Ultra-small fluorescent metal nanoclusters: synthesis and biological applications. *Nano today*. 2011, vol. 6, no. 4, pp. 401–418. Available from DOI: [10.1016/j.nantod.2011.06.004](https://doi.org/10.1016/j.nantod.2011.06.004).
- [19] LU, Yizhong; CHEN, Wei. Sub-nanometre sized metal clusters: from synthetic challenges to the unique property discoveries. *Chemical Society Reviews*. 2012, vol. 41, no. 9, pp. 3594–3623. Available from DOI: [10.1039/C2CS15325D](https://doi.org/10.1039/C2CS15325D).
- [20] LI, Gao; JIN, Rongchao. Atomically precise gold nanoclusters as new model catalysts. *Accounts of chemical research*. 2013, vol. 46, no. 8, pp. 1749–1758. Available from DOI: [10.1039/C2CS15325D](https://doi.org/10.1039/C2CS15325D).
- [21] SHARIFI, Shahriar; BEHZADI, Shahed; LAURENT, Sophie; FORREST, M Laird; STROEVE, Pieter; MAHMOUDI, Morteza. Toxicity of nanomaterials. *Chemical Society Reviews*. 2012, vol. 41, no. 6, pp. 2323–2343. Available from DOI: [10.1039/C1CS15188F](https://doi.org/10.1039/C1CS15188F).
- [22] LYNCH, Sean R. Iron overload: prevalence and impact on health. *Nutrition reviews*. 1995, vol. 53, no. 9, pp. 255–260. Available from DOI: [10.1111/j.1753-4887.1995.tb05482.x](https://doi.org/10.1111/j.1753-4887.1995.tb05482.x).

- [23] GUPTA, A. K.; GUPTA, M. Synthesis and surface engineering of iron oxide nanoparticles for biomedical applications. *Biomaterials*. 2005, vol. 26, no. 18, pp. 3995–4021. Available from DOI: [10.1016/j.biomaterials.2004.10.012](https://doi.org/10.1016/j.biomaterials.2004.10.012).
- [24] MUELLER, Nicole C.; BRAUN, Jürgen; BRUNS, Johannes; ČERNÍK, Miroslav; RISSING, Peter; RICKERBY, David; NOWACK, Bernd. Application of nanoscale zero valent iron (NZVI) for groundwater remediation in Europe. *Environmental Science and Pollution Research International*. 2012, vol. 19, no. 2, pp. 550–558. Available from DOI: [10.1007/s11356-011-0576-3](https://doi.org/10.1007/s11356-011-0576-3).
- [25] ZHANG, Hong-wang; LIU, Yi; SUN, Shou-heng. Synthesis and assembly of magnetic nanoparticles for information and energy storage applications. *Frontiers of Physics in China*. 2010, vol. 5, no. 4, pp. 347–356. Available from DOI: [10.1007/s11467-010-0104-9](https://doi.org/10.1007/s11467-010-0104-9).
- [26] TORRES GALVIS, Hirsá M; BITTER, Johannes H; DAVIDIAN, Thomas; RUITENBEEK, Matthijs; DUGULAN, A Iulian; JONG, Krijn P de. Iron particle size effects for direct production of lower olefins from synthesis gas. *Journal of the American Chemical Society*. 2012, vol. 134, no. 39, pp. 16207–16215. Available from DOI: [10.1021/ja304958u](https://doi.org/10.1021/ja304958u).
- [27] VÉKÁS, Ladislau. Ferrofluids and Magnetorheological Fluids. *Advances in Science and Technology*. 2008, vol. 54, pp. 127–136. Available from DOI: [10.4028/www.scientific.net/AST.54.127](https://doi.org/10.4028/www.scientific.net/AST.54.127).
- [28] CSETNEKI, Ildikó; FILIPCSEI, Genovéva; ZRÍNYI, Miklós. Smart Nanocomposite Polymer Membranes with On/Off Switching Control. *Macromolecules*. 2006, vol. 39, no. 5, pp. 1939–1942. Available from DOI: [10.1021/ma052189a](https://doi.org/10.1021/ma052189a).
- [29] FU, Yu; YAO, Jianjun; ZHAO, Honghao; WAN, Zhenshuai; QIU, Ying; ZHAO, Gang. Sedimentation Characterization of Gelatin Added Bidisperse Magnetorheological Fluids Containing Nanoparticles. *IOP Conference Series: Materials Science and Engineering*. 2018, vol. 392, pp. 032018. Available from DOI: [10.1088/1757-899X/392/3/032018](https://doi.org/10.1088/1757-899X/392/3/032018).
- [30] LIU, Xinhua; WANG, Lifeng; LU, He; WANG, Dongdong; CHEN, Qingqing; WANG, Zhongbin. A Study of the Effect of Nanometer Fe₃O₄ Addition on the Properties of Silicone Oil-based Magnetorheological Fluids. *Materials and Manufacturing Processes*. 2015, vol. 30, no. 2, pp. 204–209. Available from DOI: [10.1080/10426914.2014.941875](https://doi.org/10.1080/10426914.2014.941875).
- [31] KIM, Ju-Hyun; HUANG, Xing-Jiu; CHOI, Yang-Kyu. Controlled Synthesis of Gold Nanocomplex Arrays by a Combined Top-Down and Bottom-Up Approach and Their Electrochemical Behavior. *The Journal of Physical Chemistry C*. 2008, vol. 112, no. 33, pp. 12747–12753. Available from DOI: [10.1021/jp8036878](https://doi.org/10.1021/jp8036878).
- [32] HUBER, Dale L. Synthesis, properties, and applications of iron nanoparticles. *Small*. 2005, vol. 1, no. 5, pp. 482–501. Available from DOI: [10.1002/sm11.200500006](https://doi.org/10.1002/sm11.200500006).

- [33] LI, Ling; FAN, Maohong; BROWN, Robert C.; LEEUWEN, J. (Hans) Van; WANG, Jianji; WANG, Wenhua; SONG, Yonghui; ZHANG, Panyue. Synthesis, Properties, and Environmental Applications of Nanoscale Iron-Based Materials: A Review. *Critical Reviews in Environmental Science and Technology*. 2006, vol. 36, no. 5, pp. 405–431. Available from DOI: [10.1080/10643380600620387](https://doi.org/10.1080/10643380600620387).
- [34] PARK, Jongnam; AN, Kwangjin; HWANG, Yosun; PARK, Je-Geun; NOH, Han-Jin; KIM, Jae-Young; PARK, Jae-Hoon; HWANG, Nong-Moon; HYEON, Taeghwan. Ultra-large-scale syntheses of monodisperse nanocrystals. *Nature Materials*. 2004, vol. 3, no. 12, pp. 891–895. Available from DOI: [10.1038/nmat1251](https://doi.org/10.1038/nmat1251).
- [35] LU, An-Hui; SALABAS, E. L.; SCHÜTH, Ferdi. Magnetic Nanoparticles: Synthesis, Protection, Functionalization, and Application. *Angewandte Chemie International Edition*. 2007, vol. 46, no. 8, pp. 1222–1244. Available from DOI: [10.1002/anie.200602866](https://doi.org/10.1002/anie.200602866).
- [36] WU, Jun Hua; KO, Seung Pil; LIU, Hong Ling; JUNG, Myung-Hwa; LEE, Ju Hun; JU, Jae-Seon; KIM, Young Keun. Sub 5nm Fe₃O₄ nanocrystals via coprecipitation method. *Colloids and Surfaces A: Physicochemical and Engineering Aspects*. 2008, vol. 313-314, pp. 268–272. Available from DOI: [10.1016/j.colsurfa.2007.04.108](https://doi.org/10.1016/j.colsurfa.2007.04.108).
- [37] CHOI, C. J; TOLOCHKO, O; KIM, B. K. Preparation of iron nanoparticles by chemical vapor condensation. *Materials Letters*. 2002, vol. 56, no. 3, pp. 289–294. Available from DOI: [10.1016/S0167-577X\(02\)00457-3](https://doi.org/10.1016/S0167-577X(02)00457-3).
- [38] FRACASSO, Giulio et al. Nanoaggregates of iron poly-oxo-clusters obtained by laser ablation in aqueous solution of phosphonates. *Journal of Colloid and Interface Science*. 2018, vol. 522, pp. 208–216. Available from DOI: [10.1016/j.jcis.2018.03.065](https://doi.org/10.1016/j.jcis.2018.03.065).
- [39] CASTRO, Hemerson PS et al. Synthesis and characterisation of fluorescent carbon nanodots produced in ionic liquids by laser ablation. *Chemistry–A European Journal*. 2016, vol. 22, no. 1, pp. 138–143. Available from DOI: [10.1002/chem.201503286](https://doi.org/10.1002/chem.201503286).
- [40] FOJTIK, Anton; HENGLEIN, Arnim. Laser ablation of films and suspended particles in a solvent: formation of cluster and colloid solutions. *Berichte der Bunsen-Gesellschaft*. 1993, vol. 97, no. 2, pp. 252–254.
- [41] PATIL, PP; PHASE, DM; KULKARNI, SA; GHASIAS, SV; KULKARNI, SK; KANETKAR, SM; OGALE, SB; BHIDE, VG. Pulsed-laser-induced reactive quenching at liquid-solid interface: Aqueous oxidation of iron. *Physical review letters*. 1987, vol. 58, no. 3, pp. 238. Available from DOI: [10.1103/PhysRevLett.58.238](https://doi.org/10.1103/PhysRevLett.58.238).

- [42] ZHANG, Dongshi; GÖKCE, Bilal; BARCIKOWSKI, Stephan. Laser synthesis and processing of colloids: fundamentals and applications. *Chemical reviews*. 2017, vol. 117, no. 5, pp. 3990–4103. Available from DOI: [10.1021/acs.chemrev.6b00468](https://doi.org/10.1021/acs.chemrev.6b00468).
- [43] LETZEL, Alexander et al. Time and Mechanism of Nanoparticle Functionalization by Macromolecular Ligands during Pulsed Laser Ablation in Liquids. *Langmuir*. 2019, vol. 35, no. 8, pp. 3038–3047. Available from DOI: [10.1021/acs.langmuir.8b01585](https://doi.org/10.1021/acs.langmuir.8b01585).
- [44] SHELDON, Roger A. Fundamentals of green chemistry: efficiency in reaction design. *Chemical Society Reviews*. 2012, vol. 41, no. 4, pp. 1437–1451. Available from DOI: [10.1039/C1CS15219J](https://doi.org/10.1039/C1CS15219J).
- [45] BARCIKOWSKI, Stephan; AMENDOLA, Vincenzo; MARZUN, Galina; REHBOCK, Christoph; REICHENBERGER, Sven; ZHANG, Dongshi; GÖKCE, Bilal. Handbook of laser synthesis of colloids. 2016. Available from DOI: [10.17185/dupublico/41087](https://doi.org/10.17185/dupublico/41087).
- [46] MAURER, Michael J. Relaxation Model for Heat Conduction in Metals. *Journal of Applied Physics*. 1969, vol. 40, no. 13, pp. 5123–5130. Available from DOI: [10.1063/1.1657362](https://doi.org/10.1063/1.1657362).
- [47] EL-SAYED, Mostafa A. Some Interesting Properties of Metals Confined in Time and Nanometer Space of Different Shapes. *Accounts of Chemical Research*. 2001, vol. 34, no. 4, pp. 257–264. Available from DOI: [10.1021/ar960016n](https://doi.org/10.1021/ar960016n).
- [48] PYATENKO, Alexander; WANG, Hongqiang; KOSHIZAKI, Naoto; TSUJI, Takeshi. Mechanism of pulse laser interaction with colloidal nanoparticles. *Laser & Photonics Reviews*. 2013, vol. 7, no. 4, pp. 596–604. Available from DOI: [10.1002/lpor.201300013](https://doi.org/10.1002/lpor.201300013).
- [49] PYATENKO, A.; SHIMOKAWA, K.; YAMAGUCHI, M.; NISHIMURA, O.; SUZUKI, M. Synthesis of silver nanoparticles by laser ablation in pure water. *Applied Physics A*. 2004, vol. 79, no. 4, pp. 803–806. Available from DOI: [10.1007/s00339-004-2841-5](https://doi.org/10.1007/s00339-004-2841-5).
- [50] STRASSER, Michael; SETOURA, Kenji; LANGBEIN, Uwe; HASHIMOTO, Shuichi. Computational Modeling of Pulsed Laser-Induced Heating and Evaporation of Gold Nanoparticles. *The Journal of Physical Chemistry C*. 2014, vol. 118, no. 44, pp. 25748–25755. Available from DOI: [10.1021/jp508316v](https://doi.org/10.1021/jp508316v).
- [51] MAXIMOVA, Ksenia; ARISTOV, Andrei; SENTIS, Marc; KABASHIN, Andrei V. Size-controllable synthesis of bare gold nanoparticles by femtosecond laser fragmentation in water. *Nanotechnology*. 2015, vol. 26, no. 6, pp. 065601. Available from DOI: [10.1088/0957-4484/26/6/065601](https://doi.org/10.1088/0957-4484/26/6/065601).

- [52] TANGEYSH, Behzad; MOORE TIBBETTS, Katharine; ODHNER, Johanan H.; WAYLAND, Bradford B.; LEVIS, Robert J. Gold Nanoparticle Synthesis Using Spatially and Temporally Shaped Femtosecond Laser Pulses: Post-Irradiation Auto-Reduction of Aqueous $[AuCl_4]^-$. *The Journal of Physical Chemistry C*. 2013, vol. 117, no. 36, pp. 18719–18727. Available from DOI: [10.1021/jp4056494](https://doi.org/10.1021/jp4056494).
- [53] TAKAMI, Akinori; KURITA, Hideaki; KODA, Seiichiro. Laser-induced size reduction of noble metal particles. *The Journal of Physical Chemistry B*. 1999, vol. 103, no. 8, pp. 1226–1232. Available from DOI: [10.1021/jp983503o](https://doi.org/10.1021/jp983503o).
- [54] PYATENKO, Alexander; YAMAGUCHI, Munehiro; SUZUKI, Masaaki. Mechanisms of size reduction of colloidal silver and gold nanoparticles irradiated by Nd: YAG laser. *The Journal of Physical Chemistry C*. 2009, vol. 113, no. 21, pp. 9078–9085. Available from DOI: [10.1021/jp808300q](https://doi.org/10.1021/jp808300q).
- [55] ISHIKAWA, Yoshie; KOSHIZAKI, Naoto; PYATENKO, Alexander. Submicrometer-Sized Spherical Iron Oxide Particles Fabricated by Pulsed Laser Melting in Liquid. *Electronics and Communications in Japan*. 2016, vol. 99, no. 11, pp. 37–42. Available from DOI: [10.1002/ecj.11898](https://doi.org/10.1002/ecj.11898).
- [56] REHBOCK, Christoph; JAKOBI, Jurij; GAMRAD, Lisa; VAN DER MEER, Selina; TIEDEMANN, Daniela; TAYLOR, Ulrike; KUES, Wilfried; RATH, Detlef; BARCIKOWSKI, Stephan. Current state of laser synthesis of metal and alloy nanoparticles as ligand-free reference materials for nano-toxicological assays. *Beilstein journal of nanotechnology*. 2014, vol. 5, no. 1, pp. 1523–1541. Available from DOI: [10.3762/bjnano.5.165](https://doi.org/10.3762/bjnano.5.165).
- [57] *Javascript Mie scattering calculator* [<https://saviot.cnrs.fr/mie/index.en.html>]. Accessed: 2019-04-22.
- [58] BERNE, Bruce J; PECORA, Robert. *Dynamic light scattering: with applications to chemistry, biology, and physics*. Courier Corporation, 2000. ISBN 0-486-41155-9.
- [59] BOCCACCINI, Aldo R; BIEST, Omer van der; TALBOT, Jan B. Electrophoretic Deposition, Fundamentals and Applications: Proceedings of the International Symposium. In: 2002. ISBN 1-56677-345-8.
- [60] FREY, Natalie A; PENG, Sheng; CHENG, Kai; SUN, Shouheng. Magnetic nanoparticles: synthesis, functionalization, and applications in bioimaging and magnetic energy storage. *Chemical Society Reviews*. 2009, vol. 38, no. 9, pp. 2532–2542. Available from DOI: [10.1039/B815548H](https://doi.org/10.1039/B815548H).
- [61] ATUL; KUMAR, Manish; SHARMA, Anjna; MAURYA, Indresh Kumar; THAKUR, Alpana; KUMAR, Sunil. Synthesis of ultra small iron oxide and doped iron oxide nanostructures and their antimicrobial activities. *Journal of Taibah University for Science*. 2019, vol. 13, no. 1, pp. 280–285. Available from DOI: [10.1080/16583655.2019.1565437](https://doi.org/10.1080/16583655.2019.1565437).

- [62] YUVAKKUMAR, R; ELANGO, V; RAJENDRAN, V; KANNAN, N. Preparation and characterization of zero valent iron nanoparticles. *Digest journal of nanomaterials and biostructures*. 2011, vol. 6, no. 4, pp. 1771–1776. Available from DOI: [10.1002/vjch.201800018](https://doi.org/10.1002/vjch.201800018).
- [63] CHENG, Kang; GU, Bang; LIU, Xiaoliang; KANG, Jincan; ZHANG, Qinghong; WANG, Ye. Direct and highly selective conversion of synthesis gas into lower olefins: design of a bifunctional catalyst combining methanol synthesis and carbon–carbon coupling. *Angewandte chemie international edition*. 2016, vol. 55, no. 15, pp. 4725–4728. Available from DOI: [10.1002/anie.201601208](https://doi.org/10.1002/anie.201601208).
- [64] CAO, Shao-Wen; ZHU, Ying-Jie; CHANG, Jiang. Fe₃ O₄ polyhedral nanoparticles with a high magnetization synthesized in mixed solvent ethylene glycol–water system. *New Journal of Chemistry*. 2008, vol. 32, no. 9, pp. 1526–1530. Available from DOI: [10.1039/B719436F](https://doi.org/10.1039/B719436F).
- [65] DONATE-BUENDIA, Carlos; TORRES-MENDIETA, Rafael; PYATENKO, Alexander; FALOMIR, Eva; FERNÁNDEZ-ALONSO, Mercedes; MÍNGUEZ-VEGA, Gladys. Fabrication by laser irradiation in a continuous flow jet of carbon quantum dots for fluorescence imaging. *ACS omega*. 2018, vol. 3, no. 3, pp. 2735–2742. Available from DOI: [10.1021/acsomega.7b02082](https://doi.org/10.1021/acsomega.7b02082).
- [66] AMENDOLA, Vincenzo; RIELLO, Pietro; MENEGHETTI, Moreno. Magnetic nanoparticles of iron carbide, iron oxide, iron@ iron oxide, and metal iron synthesized by laser ablation in organic solvents. *The journal of physical chemistry C*. 2010, vol. 115, no. 12, pp. 5140–5146. Available from DOI: [10.1021/jp109371m](https://doi.org/10.1021/jp109371m).
- [67] KIM, Eun-Ju; KIM, Jae-Hwan; AZAD, Abdul-Majeed; CHANG, Yoon-Seok. Facile synthesis and characterization of Fe/FeS nanoparticles for environmental applications. *ACS applied materials & interfaces*. 2011, vol. 3, no. 5, pp. 1457–1462. Available from DOI: [10.1021/am200016v](https://doi.org/10.1021/am200016v).
- [68] DONG, Hailong; ROMING, Marcus; FELDMANN, Claus. Unexpected fluorescence of polyols and PEGylated nanoparticles derived from carbon dot formation. *Particle and Particle Systems Characterization*. 2015, vol. 32, no. 4, pp. 467–475. Available from DOI: [10.1002/ppsc.201400173](https://doi.org/10.1002/ppsc.201400173).
- [69] PAIK, Sankar Prasad; GHATAK, Sumanta Kumar; DEY, Debarati; SEN, Kamalika. Poly (ethylene glycol) vesicles: self-assembled site for luminescence generation. *Analytical chemistry*. 2012, vol. 84, no. 17, pp. 7555–7561. Available from DOI: [10.1021/ac301731x](https://doi.org/10.1021/ac301731x).
- [70] TORRES-MENDIETA, R; MONDRAGÓN, R; JULIÁ, E; MENDOZA-YERO, O; CORDONCILLO, E; LANCIS, J; MÍNGUEZ-VEGA, G. Fabrication of gold nanoparticles in Therminol VP-1 by laser ablation and fragmentation with fs pulses. *Laser Physics Letters*. 2014, vol. 11, no. 12, pp. 126001. Available from DOI: [10.1088/1612-2011/11/12/126001](https://doi.org/10.1088/1612-2011/11/12/126001).

- [71] KULKARNI, Vitthal S. *Handbook of non-invasive drug delivery systems: science and technology*. Elsevier, 2009. ISBN 978-0-8155-2025-2.
- [72] GRUMEZESCU, Alexandru Mihai. *Multifunctional systems for combined delivery, biosensing and diagnostics*. William Andrew, 2017. ISBN 978-0-323-52725-5.
- [73] SHOSTAK, K.; ABELSON, John N.; COLOWICK, S.P.; SIMON, M.I. *Cumulative Subject Index*. Academic Press, 1998. Cumulative Subject Index [to] Methods in Enzymology, no. v. 263-264;v. 266-289. ISBN 9780121821869. Available also from: <https://books.google.cz/books?id=cHdFMQAACAAJ>.
- [74] WU, Shiliang; YANG, Hongwei; HU, Jun; SHEN, Dekui; ZHANG, Huiyan; XIAO, Rui. The miscibility of hydrogenated bio-oil with diesel and its applicability test in diesel engine: A surrogate (ethylene glycol) study. *Fuel Processing Technology*. 2017, vol. 161, pp. 162–168. Available from DOI: [10.1016/j.fuproc.2017.03.022](https://doi.org/10.1016/j.fuproc.2017.03.022).
- [75] MOTIN, Md Abdul; MIA, MA Hafiz; ISLAM, AKM Nasimul. Thermodynamic properties of Sodium Dodecyl Sulfate aqueous solutions with Methanol, Ethanol, n-Propanol and iso-Propanol at different temperatures. *Journal of Saudi Chemical Society*. 2015, vol. 19, no. 2, pp. 172–180. Available from DOI: [10.1016/j.jscs.2012.01.009](https://doi.org/10.1016/j.jscs.2012.01.009).
- [76] YAMAGUCHI, Noriko; SATO, Mari. Dipole moment of poly (ethylene oxide) in solution and its dependence on molecular weight and temperature. *Polymer journal*. 2009, vol. 41, no. 8, pp. 588. Available from DOI: [10.1295/polymj.PJ2008232](https://doi.org/10.1295/polymj.PJ2008232).
- [77] RUDAN-TASIC, Darja; KLOFUTAR, Cveto. Apparent specific polarization and dipole moment of some poly (oxyethylene) glycols in 1, 4-dioxane and benzene solutions at 298.15 K. *Monatshfte für Chemie/Chemical Monthly*. 2005, vol. 136, no. 7, pp. 1171–1182. Available from DOI: [10.1007/s00706-005-0323-x](https://doi.org/10.1007/s00706-005-0323-x).
- [78] TILAKI, RM; MAHDAVI, SM, et al. Size, composition and optical properties of copper nanoparticles prepared by laser ablation in liquids. *Applied Physics A*. 2007, vol. 88, no. 2, pp. 415–419. Available from DOI: [10.1007/s00339-007-4000-2](https://doi.org/10.1007/s00339-007-4000-2).
- [79] PFLEGER, Jiri; SMEJKAL, Petr; VLCKOVA, Blanka; SLOUF, Miroslav. Preparation of Ag nanoparticles by two-wavelength laser ablation and fragmentation. In: *Advanced Organic and Inorganic Optical Materials*. 2003, vol. 5122, pp. 198–206. Available from DOI: [10.1117/12.515724](https://doi.org/10.1117/12.515724).
- [80] TORRES-MENDIETA, Rafael; HAVELKA, Ondřej; URBÁNEK, Michal; CVEK, Martin; WACŁAWEK, Stanisław; PADIL, Vinod Vellora Thekkae; JAŠÍKOVÁ, Darina; KOTEK, Michal; ČERNÍK, Miroslav. Laser-assisted synthesis of Fe-Cu oxide nanocrystals. *Applied Surface Science*. 2019, vol. 469, pp. 1007–1015. Available from DOI: [10.1016/j.apsusc.2018.11.058](https://doi.org/10.1016/j.apsusc.2018.11.058).

- [81] WU, Wei; HE, Quanguo; JIANG, Changzhong. Magnetic iron oxide nanoparticles: synthesis and surface functionalization strategies. *Nanoscale research letters*. 2008, vol. 3, no. 11, pp. 397. Available from DOI: [10.1007/s11671-008-9174-9](https://doi.org/10.1007/s11671-008-9174-9).
- [82] CHIRITA, M; GROZESCU, I; TAUBERT, L, et al. Fe₂O₃-nanoparticles, physical properties and their photochemical and photoelectrochemical applications. *Chemical Bulletin*. 2009, vol. 54, no. 68, pp. 1–8. Available from DOI: [10.1.1.559.542](https://doi.org/10.1.1.559.542).